

UNCLASSIFIED

AD NUMBER
AD403338
NEW LIMITATION CHANGE
TO Approved for public release, distribution unlimited
FROM Distribution authorized to U.S. Gov't. agencies and their contractors; Administrative/Operational Use; JAN 1963. Other requests shall be referred to Air Force Aeronautical Systems Division, Attn: Materials and Processes, Wright-Patterson AFB, OH 45433.
AUTHORITY
afwal ltr, 6 Jul 1981

THIS PAGE IS UNCLASSIFIED



TECHNICAL DOCUMENTARY REPORT
NO. ASD-TDR-62-202, Part II
CONTRACT AF 33(616)-7765

HIGH TEMPERATURE INORGANIC STRUCTURAL
COMPOSITE MATERIALS
JANUARY, 1963



**THE CERAMIC ENGINEERING DEPARTMENT
OF
MISSISSIPPI STATE UNIVERSITY**

40-738

NO OTS

NOTICES

When Government drawings, specifications, or other data are used for any purpose other than in connection with a definitely related Government procurement operation, the United States Government thereby incurs no responsibility nor any obligation whatsoever; and the fact that the Government may have formulated, furnished, or in any way supplied the said drawings, specifications, or other data, is not to be regarded by implication or otherwise as in any manner licensing the holder or any other person or corporation, or conveying any rights or permission to manufacture, use, or sell any patented invention that may in any way be related thereto.

ASTIA release to OTS not authorized.

Qualified requesters may obtain copies of this report from the Armed Services Technical Information Agency, (ASTIA), Arlington Hall Station, Arlington 12, Virginia.

Copies of this report should not be returned to the Aeronautical Systems Division unless return is required by security considerations, contractual obligations, or notice on a specific document.

ASD-TDR-62-202
PART II

HIGH TEMPERATURE INORGANIC STRUCTURAL
COMPOSITE MATERIALS

TECHNICAL DOCUMENTARY REPORT NO. ASD-TDR-62-202, Pt. II
JANUARY 1963

Directorate of Materials and Processes
Aeronautical Systems Division
Air Force Systems Command
United States Air Force
Wright-Patterson Air Force Base, Ohio

Project 7340, Task 734003

(Prepared under Contract AF 33(616)-7765 by Department of Ceramic
Engineering, Mississippi State University, State College, Mississippi
by A.G. Wehr, W.B. Hall, and J.H. Lauchner, authors.)

FOREWORD

This report was prepared in the Department of Ceramic Engineering at Mississippi State University under USAF Contract No. AF 33(616)-7765. This contract was initiated under Project No. 7340, "Nonmetallic and Composite Materials," Task No. 734003, "Structural Plastics and Composites".

It was administered under the direction of the Directorate of Materials and Processes, Aeronautical Systems Division, with Mr. Frank Fechek acting as Project Engineer.

This report covers the period of work from December 14, 1961 to December 15, 1962.

Personnel participating in the research included Allan G. Wehr, principal investigator, William B. Hall, and Julian H. Lauchner.

ABSTRACT

Two phosphate bonded matrix materials for a composite system were studied. Polymorphism of the aluminum phosphate was responsible for wide variance in physical properties of the matrix material. Composites formed of these matrix materials reinforced with E-glass fibers had strengths two and one-half times that of matrix alone. Studies were conducted of the effect of corrosion on the fibers by the phosphate material. Corrosion varied as method of processing with wet layup specimens being more corrosive and dry pressed specimens being least corrosive.

Boron fibers were investigated as a possible reinforcement material. Boron fibers were more corrosive resistant than glass fibers, but also were more brittle, presenting a processing problem. Microscopic examination of the fibers revealed several interesting structural habits of these fibers. Strength properties of the composites were determined on an automatic stress-strain apparatus designed and built specifically for that purpose.

This report has been reviewed and is approved.

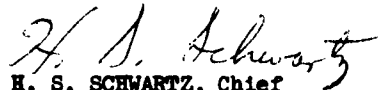

H. S. SCHWARTZ, Chief
Plastics & Composites Branch
Nonmetallic Materials Laboratory
Directorate of Materials & Processes

TABLE OF CONTENTS

	Page
I. INTRODUCTION.....	1
II. MATRIX DEVELOPMENT.....	2
III. COMPOSITES.....	7
A. Amblate	7
B. LiF E-Glass Composite.....	21
IV. E-18 POLYMORPHIC STUDY.....	31
A. Detection and Identification of the Crystallographic Inversions Occurring in E-18 Oxide-Phosphate Bonded Specimens	31
B. X-ray Diffraction Studies of E-18 Oxide-Phosphate Bonded Material.....	32
V. EQUIPMENT.....	34
A. Automatic Stress-Strain.....	34
B. Nitriding System.....	42
VI. DISCUSSION OF RESULTS.....	44
VII. CONCLUSIONS.....	46
VIII. REFERENCES	47
APPENDIX	60

LIST OF ILLUSTRATIONS

Figure	Page
1. Matrix Processing.....	4
2. Micrograph of Amblate Sintered at 300°F for One Hour.....	5
3. Micrograph of Amblate Sintered at 1200°F for One Hour.....	5
4. Micrograph of Amblate Sintered at 1200°F for Two Hours	6
5. Micrograph of Amblate Sintered at 1200°F for Two Hours	6
6. Amblate - E-glass Fiber Pellet Reacted at 400°F...	8
7. Amblate - E-glass Fiber Pellet Reacted at 550°F...	8
8. Amblate E-glass Fiber Pellet Reacted at 650°F.....	9
9. Amblate E-glass Fiber Pellet Reacted at 700°F.....	9
10. Stress-Strain Curves for Amblate - Untreated E-glass Composites	10
11. Stress-Strain Curves for Amblate - Untreated E-glass Composites	11
12. Stress-Strain Curves for Amblate - Untreated E-glass Composites	12
13. Stress-Strain Curves for Amblate - Untreated E-glass Composites	13
14. Stress-Strain Curves for Amblate- Desized E-glass Composites	14
15. Stress-Strain Curves for Amblate - Desized E-glass Composites	15
16. Stress-Strain Curves for Amblate - Untreated N-glass Composites	16
17. Stress-Strain Curves for Amblate - Untreated N-glass Composites	17
18. Stress-Strain Curves for Amblate - Desized N-glass Composites	18

LIST OF ILLUSTRATIONS, CONT'D.

Figure

19.	Stress-Strain Curves for Amblate - Desized N-glass Composites.....	19
20.	Amblate E-Glass Dry Pressed Composite	20
21.	Porosity in LiF-E Glass Fiber Composite	22
22.	Inhomogenous Distribution of Glass Fibers in LiF-Glass Fiber Composite	22
23.	Fiber Congregation in LiF-Glass Fiber Composite	23
24.	Reaction Ring in LiF-Glass Fiber Composite	23
25.	Boron Fiber Surface	27
26.	.01 mm Reference	27
27.	Boron Fiber in E-18 Matrix (End View)	27
28.	Boron Fiber in E-18 Matrix (Side View)	27
29.	Surface of Boron Fiber in E-18 Matrix Showing Etching Stages	28
30.	Normal View of Cleavage Plane in Boron Fiber	29
31.	Amblate-B Fiber Composite	29
32.	AlPO_4 LiF-B Fiber Composite.....	30
33.	LiF-B Fiber Composite	30
34.	Modulus of Elasticity vs Temperature Phosphate Bonded Body	35
35.	Automatic Stress-Strain Equipment.....	36
36.	Balancing Bridge Circuit for Automatic Stress-Strain Curve.....	37
37.	Load vs Scale Reading Calibration Curve	39
38.	Deflection vs Scale Reading Calibration	40
39.	Engineering Stress-Strain Curve for Phosphate Bonded Speciman.....	41
40.	Nitriding Apparatus.....	43

LIST OF TABLES

	Page
I. Experimental Matrix Composition	48
II. Properties of Amblate Matrix	49
III. Modulus of Elasticity of CaF_2 and AlPO_4LiF	50
IV. Effect of Temperature on the Total Damping Time of an Oxide-Phosphate Bonded Specimen	51
IV. Effect of Temperature on the Total Damping Time of an Oxide-Phosphate Bonded Specimen, Cont'd	52
V. Detection and Evaluation of Crystallographic Inversions in E-18 Oxide Phosphate Bonded Specimens	53
VI. Phases present in E-18 Oxide-Phosphate Bonded Specimens Quenched from Various Temperatures	54
VII. Results of X-ray Diffraction Studies	55
VII. Results of X-ray Diffraction Studies, Cont'd	56
VIII. X-ray Diffraction Data for Specimen No. 2	57
IX. X-ray Diffraction Data for Specimen No. 3	58
X. X-ray diffraction Data for Specimen No. 12	59

I. INTRODUCTION

The ever increasing demand for materials which possess properties seemingly unobtainable in any single material has placed considerable emphasis upon the composite. As a direct result of higher stresses, local factors and service temperatures as might be encountered in space travel, the inorganic composite has become a necessity. Inorganic fiber reinforced plastic laminates or composites have proven to be effective at temperatures of the order of 700°F. In this composite system the high tensile strength of the fibers is utilized by maintaining a high modulus of elasticity ratio between the reinforcement and matrix phases.

The goal for this project was to develop an analogous fiber reinforced inorganic matrix composite system with a use temperature of 1000°F. The system was to be capable of low temperature deformation, and have low forming pressure and maturing temperature.

The first year's effort on this project, (Ref. 1) was mainly directed toward the development of an inorganic matrix and the evaluating of the physical properties of that material.

The body developed during the first year was designated as E-18. The composition and preliminary processing of the body is given below:

<u>Constituent</u>	<u>Weight</u>
Al ₂ O ₃	225 gms.
Co ₃ O ₄	50 gms.
ZnO	5 gms.
H ₃ PO ₄ (85% ortho phosphoric)	100 cc.

- a) Oxides ball milled for three hours.
- b) Phosphoric acid added.
- c) Heat treated at 200°C for two hours.
- d) Crushed and ball milled for 16 hours.
- e) Dried at 150°C for three hours.
- f) Particle size separation

The processed powders were evaluated in dry pressed and wet layup specimens. In general, the processing studies revealed that dry pressed bodies were dense, strong, and had a low sintering temperature, but required high forming pressure, whereas the wet layup specimens required low forming pressure but had high sintering temperature and excess porosity.

Manuscript released by authors 3 January 1963 for publication as an ASD Technical Documentary Report.

Values for the modulus of elasticity ranged from $.668 \times 10^6$ psi to 7.450×10^6 psi. Processing variables were evaluated to determine if the above variance in modulus could be correlated with processing variables, with negative results. It was theorized the variance was caused by the presence of different polymorphic phases of aluminum phosphate. Further studies on that portion of the project is covered in this report.

Results of evaluation of E-18 for inelastic deformation tendencies were promising. However, the inelastic deformation was not reproducible. It was felt that this non-reproducibility was directly related to the polymorphism of aluminum phosphate.

The values for modulus of rupture of the matrix material ranged from 390.6 psi to 5765.5 psi. The variation in strength was as large within particle size groups as between particle size groups, therefore, no conclusion was made relating strength to starting particle sizing. In addition, there was no correlation between strength and inelastic deformation, but high strength specimens usually had high modulus of elasticity.

Firing shrinkage was fairly constant with all of the inelastically deformable specimens having relatively high shrinkage. This high shrinkage substantiates the polymorphism theory as all of the different phases have different volumes.

The second year's effort was to further investigate the aluminum phosphate polymorphic phases, and to develop a phosphate bonded matrix material which did not possess the corrosiveness of E-18, and evaluate this matrix in composite systems.

II. MATRIX DEVELOPMENT

The matrix material developed in the first year of this project, E-18, had several desirable characteristics. The two major desirable characteristics being deformation tendencies and low sintering temperatures. However, E-18, an alumina phosphate body, was extremely corrosive to the inorganic fiber reinforcements. The body was so promising, however, that variations in compositions were tried in an effort to circumvent this shortcoming. This list of compositions which were formulated and evaluated are given in Table I.

The most promising of these evaluated bodies, amblate, was the one with the following composition:

Amblygonite ($\text{AlPO}_4 \cdot \text{LiF}$)	500 gms
Alumina	200 gms
Cobalt Oxide	50 gms
Zinc Oxide	5 gms
Phosphoric Acid (85%)	125 cc
Water	200 cc

Processing of the amblate bodies follows the same steps as in the processing of E-18. The powders are thoroughly mixed by ball milling for two hours. The powders are then placed in a container and the water and acid added. The mixture is stirred until homogeneity is obtained. The mixture is then placed in a furnace and reacted at 300°F. The reacted mixture is then fed through a jaw crusher for primary reduction, and then ball milled until desired particle sizing is obtained. The powders are generally ball milled for 16 hours, sieved, and oversize particles placed in the next succeeding batch to be ball milled. The sieving is accomplished utilizing Tyler screens and a rotap apparatus. The ball milling and sieving has to be continuous as these mixtures have great affinity for water, and if left exposed for any length of time, will coagulate.

The powders are then placed in a die and pressed at 3,000 pounds per square inch. The specimens are then dried and sintered at 800°F.

The raw materials used in the processing of amblate specimens are listed in Appendix I. The flow sheet for processing amblate is shown in Figure I.

Figure 2 is an electron micrograph of a dry pressed amblate specimen which was sintered at 300°F. This specimen was of interest because it had strength comparable to specimens sintered at much higher temperatures. However, as the micrograph shows, there is not much diffusion between the different grains. Figure 3 is an electron micrograph of a dry pressed amblate specimen which was sintered at 1200°F for one hour. The grain boundaries of this material are not as well defined indicating a better bonded and dense material.

The next two figures, 4 and 5, are electron micrographs of a dry pressed amblate body which was sintered at 1200°F for two hours. The specimen was densely populated with the new crystals which were forming.

In addition to the phosphate bonded matrix study, several more non-phosphate bonded bodies were briefly studied. Included in this group were simple lattice structure compositions of LiF, CaF₂, and AlPO₄LiF. Specimens for modulus of elasticity, modulus of rupture, firing temperature and deformation characteristics were prepared. All specimens were dry pressed at 3000 psi. Carbowax was used as a binder when such a material was required. The specimens were then sintered in the normal ceramic process. LiF specimens had a very short maturing range and were dropped from further consideration.

Modulus of rupture data obtained for amblate matrix specimens is given in Table 2, and modulus of elasticity values obtained for CaF₂ and AlPO₄LiF specimens are given in Table 3. F lettered specimens pertain to CaF₂ specimens while A prefixed specimens refer to AlPO₄ LiF specimens.

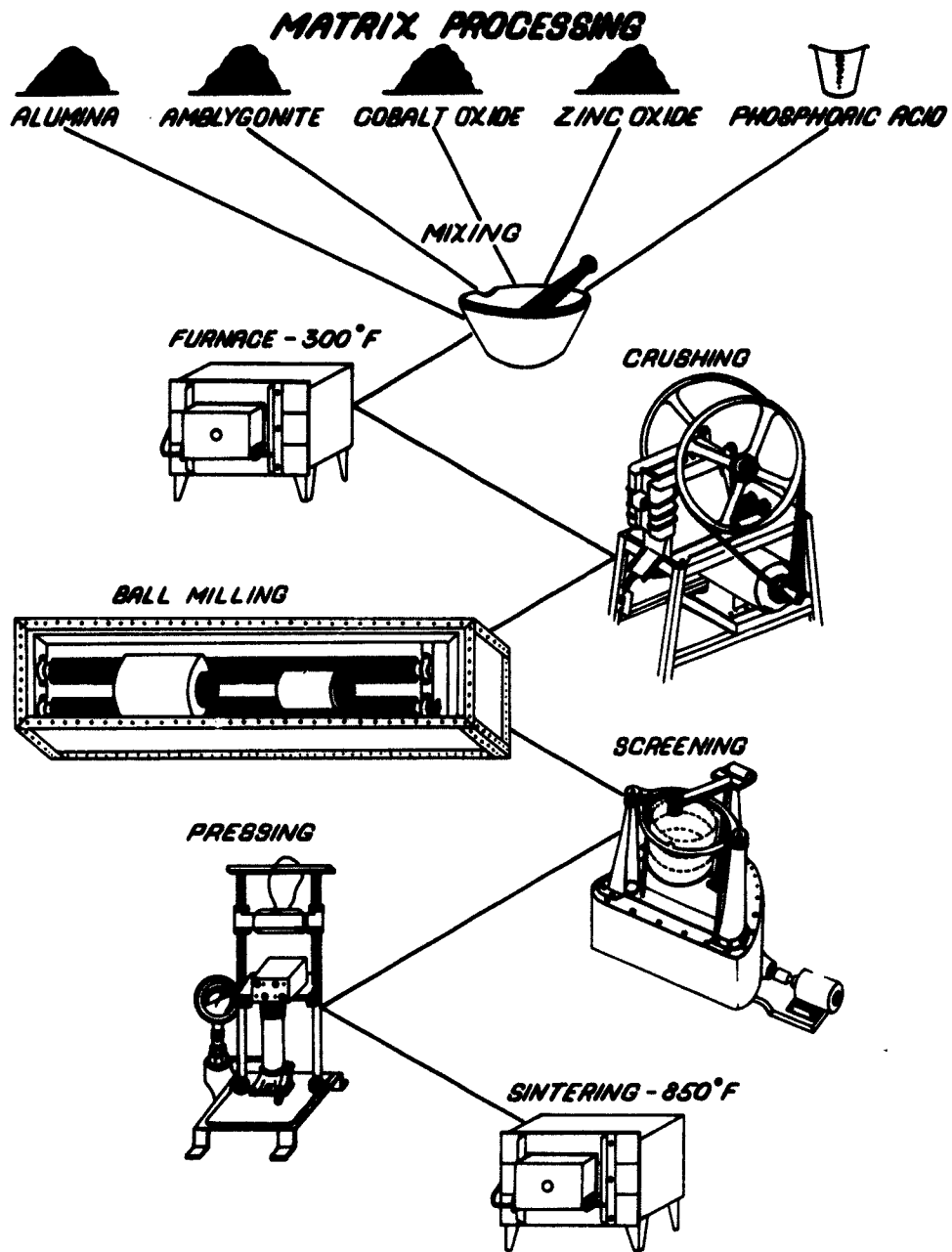


FIGURE 1



Figure 2. Amblate-Sintered 300°F for one hour. 5000X



Figure 3. Amblate-Sintered 1200°F. for one hour. 5000X



Figure 4. Amblate-Sintered 1200 F for two hours. 16,000X



Figure 5. Amblate-Sintered 1200 F for two hours. 10,000X

III. COMPOSITES

A. Amblate

Composite specimens were prepared of amblate reinforced with inorganic fibers. Specimens were prepared both by dry pressing and wet layup. The wet layup specimens were prepared by making a slurry of the amblate powders, dipping the fibers into the slurry, and then placing the coated fibers in a mold. The body was then removed from the mold, dried slowly and fired. Specimens prepared in this manner had strengths below that of the amblate matrix alone, due to fiber corrosion and bloating.

The problem of fiber corrosion in the amblate bodies was studied quite intensively. The first composites formed of amblate and E-glass by the wet layup method showed severe fiber corrosion.

A series of specimens were evaluated to determine the temperature at which the reaction took place. The amblate fiber composites, PVA as binder, were molded into pellets 1/4" thick by 3/4" diameter, and dried at 150°F. The specimens were then fired, with one specimen being removed at each selected maximum exposure temperature. The specimens were all exposed for thirty minutes at the maximum temperature. The specimens were allowed to cool, then sectioned, ground, and polished. The specimens were then examined under the Lietz microscope. Incident, incident polarized, and oblique illumination was used for observation.

The fibers, as shown in Figures 6 through 9, were easily seen both microscopically and macroscopically. The fibers appeared strong and unreacted. No reaction rings could be observed in any specimen. The matrix and fibers had good bonding, better than any observed to date.

The composite bars formed by wet layup, however, continued to exhibit porosity and corrosion above that of the pellets.

Dry pressed specimens were prepared by placing a thin layer of amblate powders in a die followed by a layer of fibers placed by hand, and continuing this cycle until the die cavity was full. The specimen was open pressed at 3000 psi, dried, and fired. Figures 10 through Figure 19 shows the results of the evaluation of the dry pressed specimens at 900°F. Fibers processed in the amblate matrix as described above were all in excellent shape as shown in Figure 20. The fibers did not have a strong bond with the matrix, however.

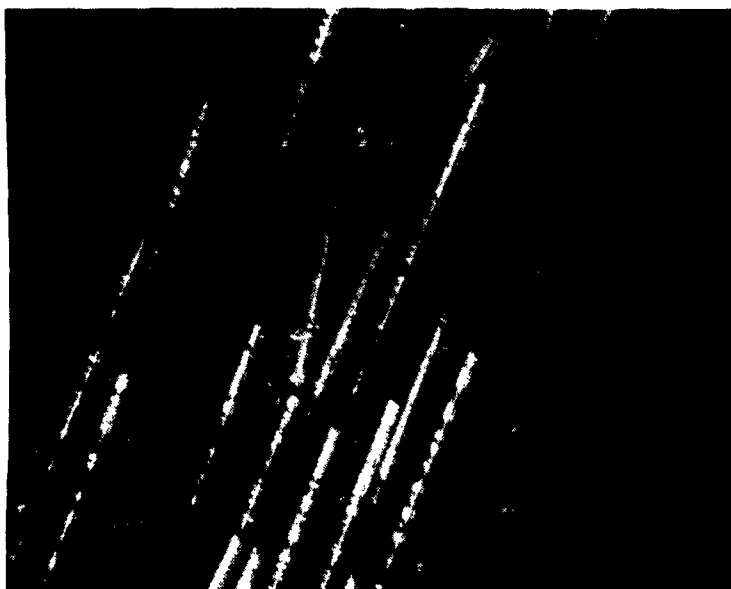


Figure 6. Reacted at 400^oF. X150

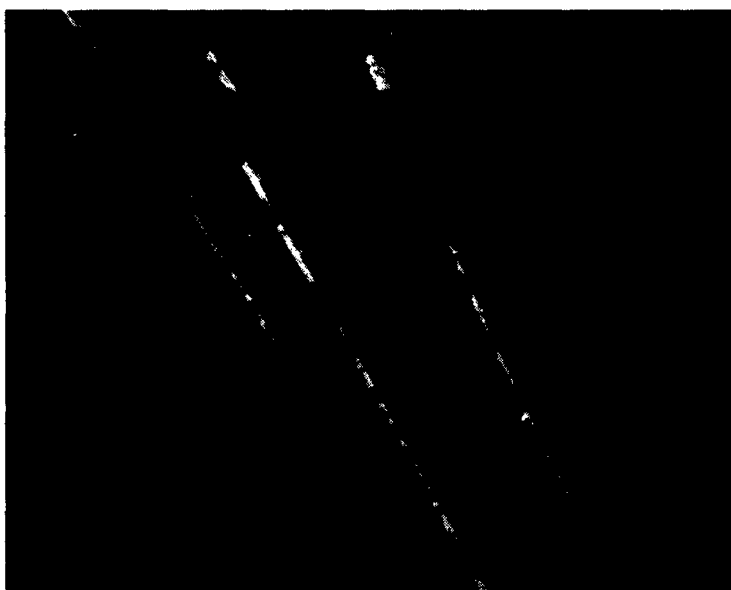


Figure 7. Reacted at 550^oF. X150

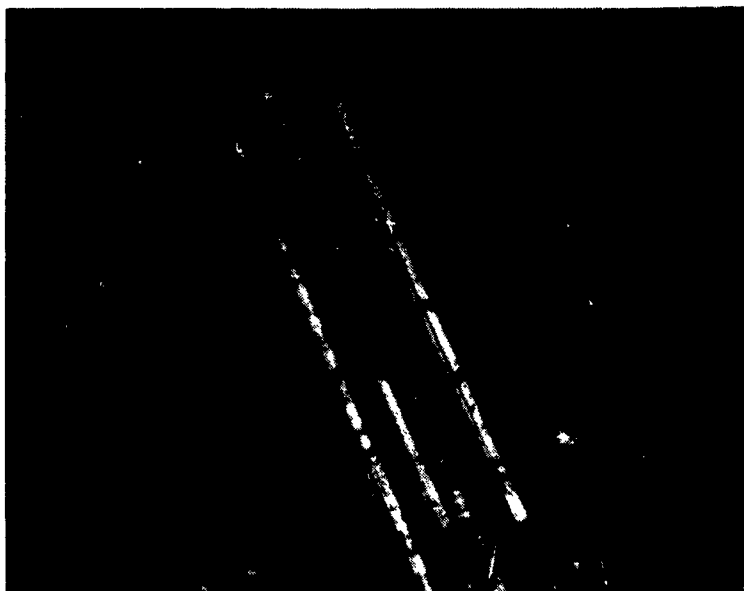


Figure 8. Reacted at 650^oF. X150

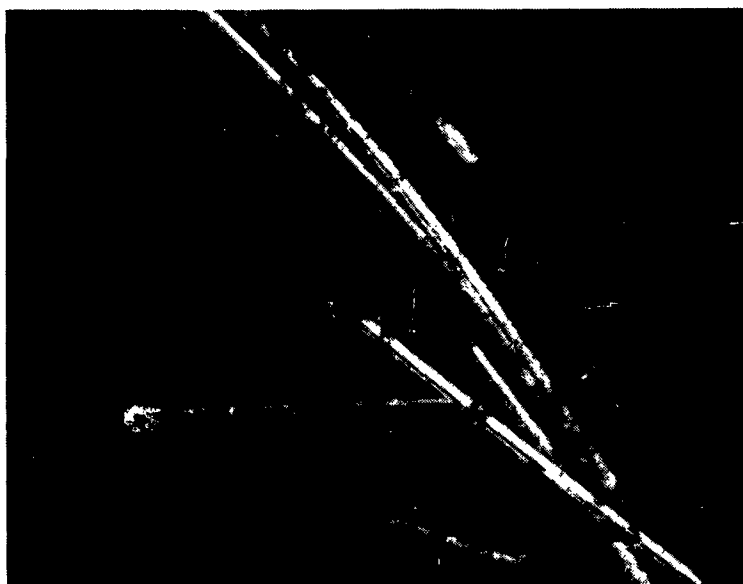


Figure 9. Reacted at 700^oF. X150

***STRESS-STRAIN CURVES FOR AMBLATE-
UNTREATED "E" GLASS COMPOSITE***

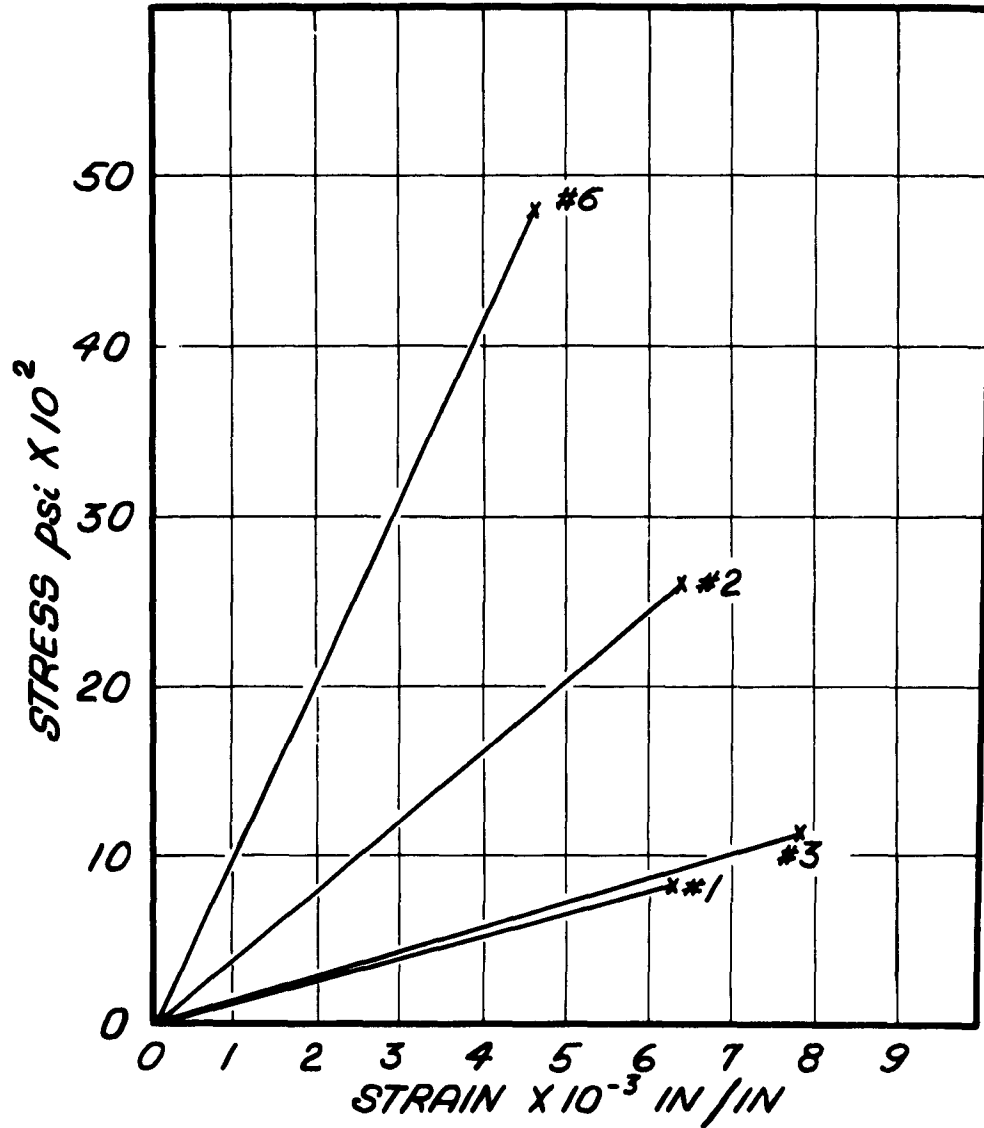


FIGURE 10

**STRESS-STRAIN CURVES FOR ANBLATE-
UNTREATED 'E' GLASS COMPOSITE**

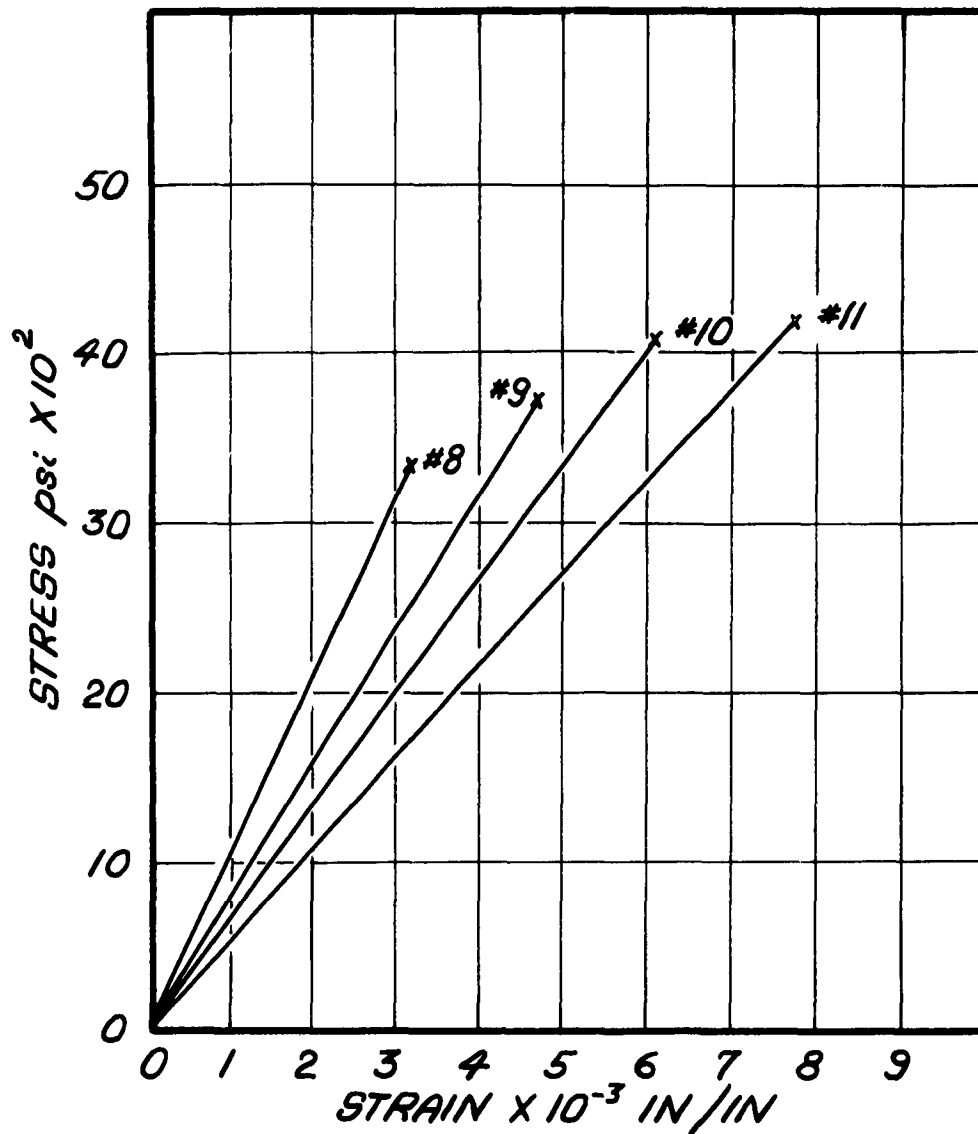


FIGURE 11

**STRESS-STRAIN CURVES FOR AMBLATE-
UNTREATED 'E' GLASS COMPOSITE**

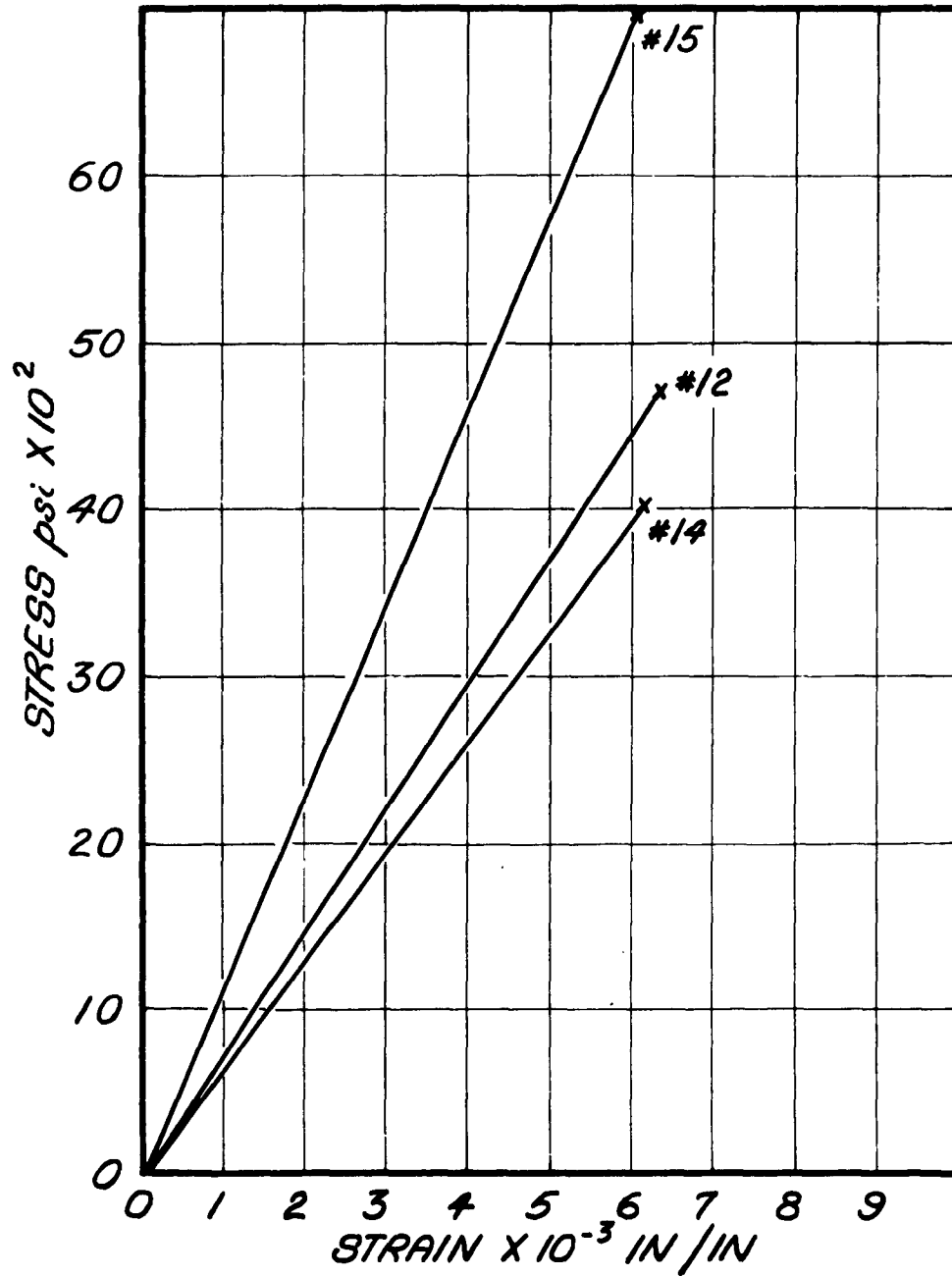


FIGURE 12

***STRESS-STRAIN CURVES FOR AMBLATE-
UNTREATED 'E' GLASS COMPOSITE***

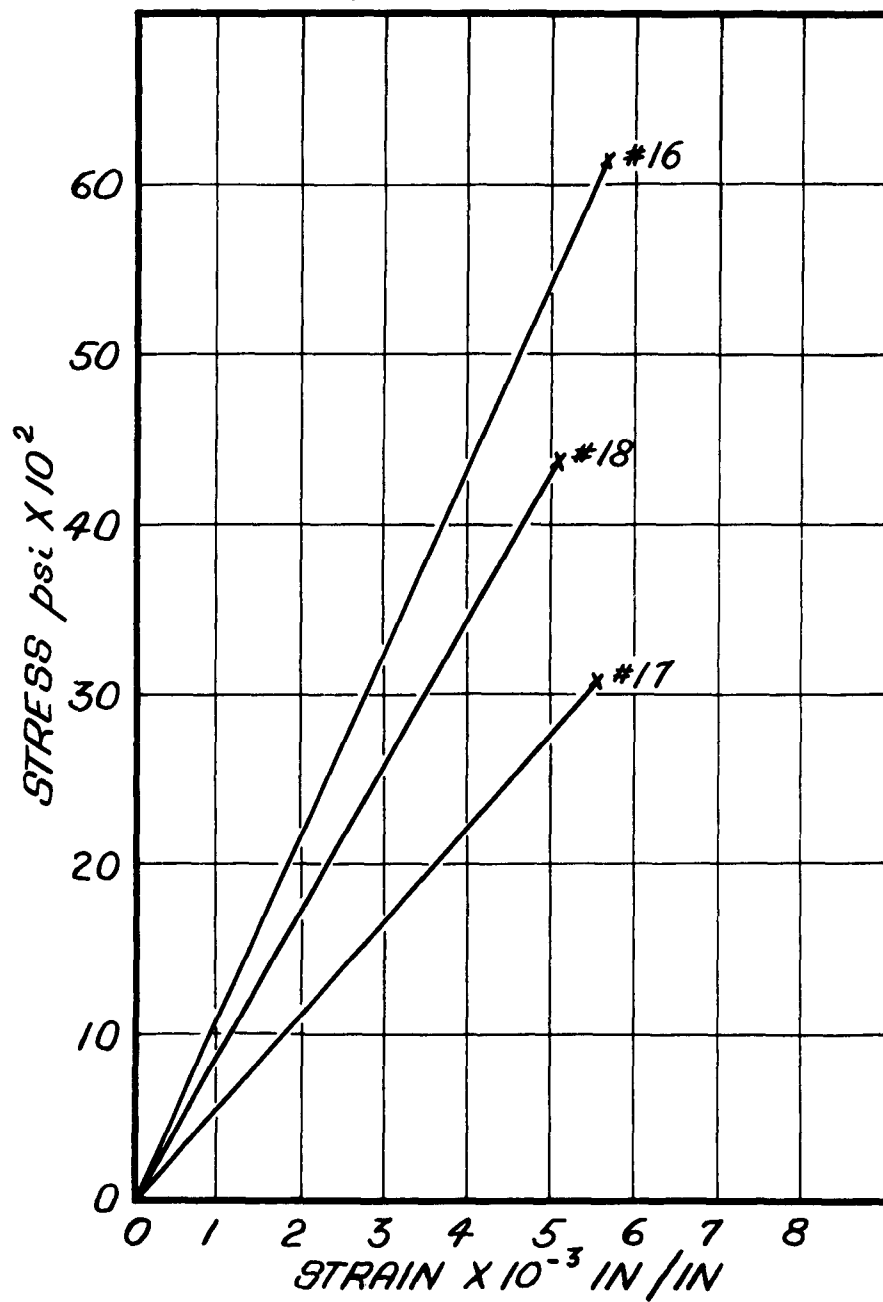


FIGURE 13

**STRESS-STRAIN CURVES FOR AMBLATE-
DESIZED *E* GLASS COMPOSITE**

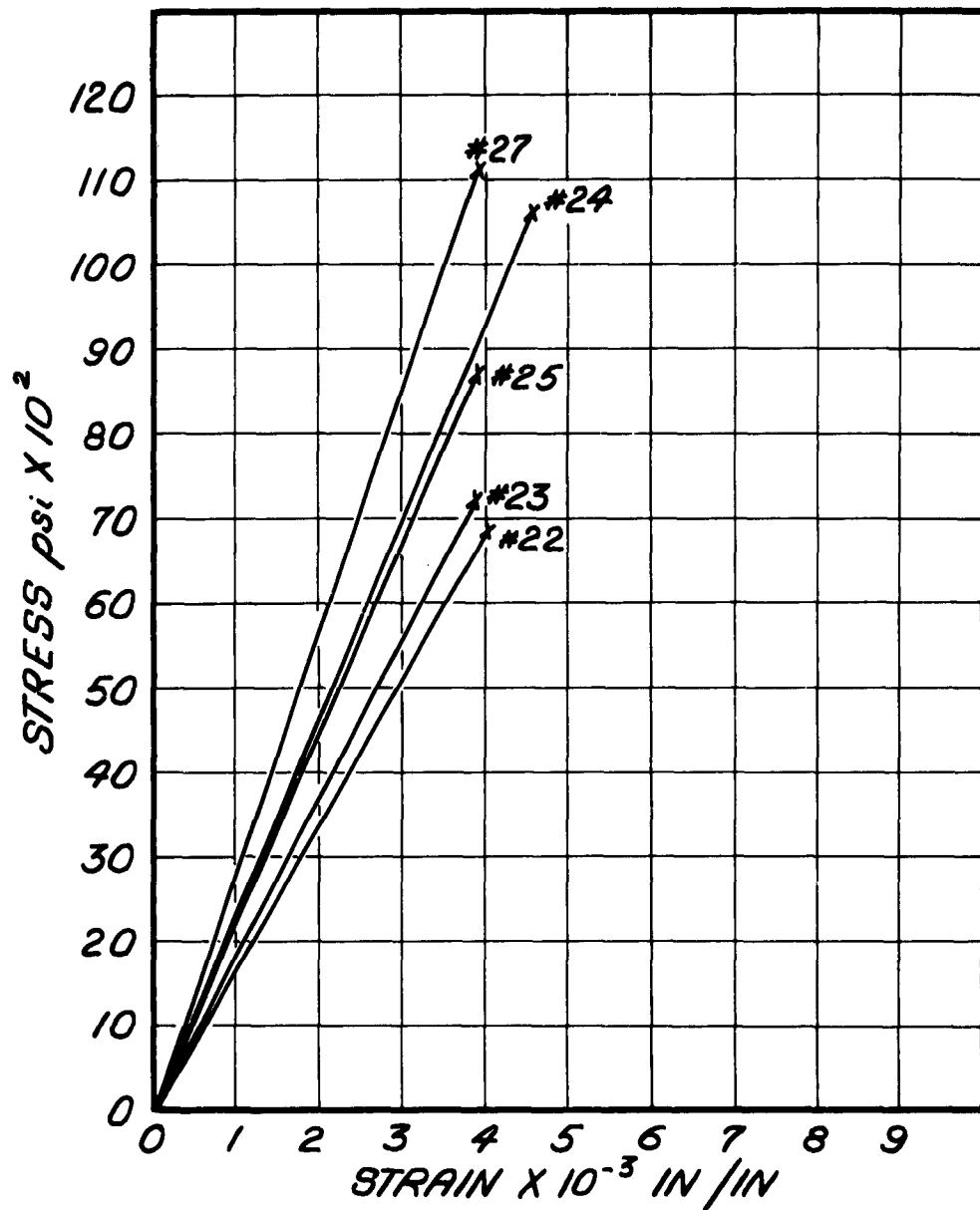


FIGURE 14

***STRESS-STRAIN CURVES FOR AMBLATE-
DESIZED 'E' GLASS COMPOSITE***

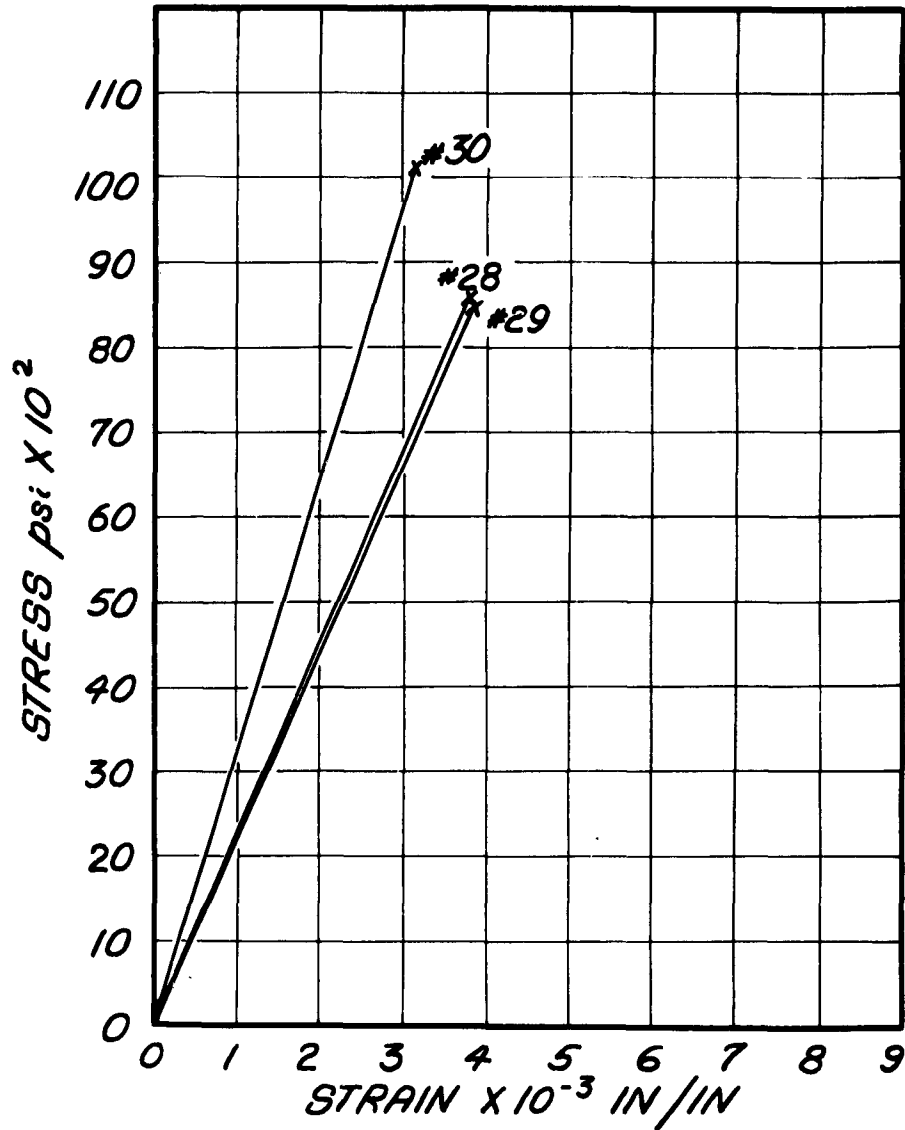


FIGURE 15

***STRESS-STRAIN CURVES FOR AMBLATE-
UNTREATED 'N' GLASS COMPOSITE***

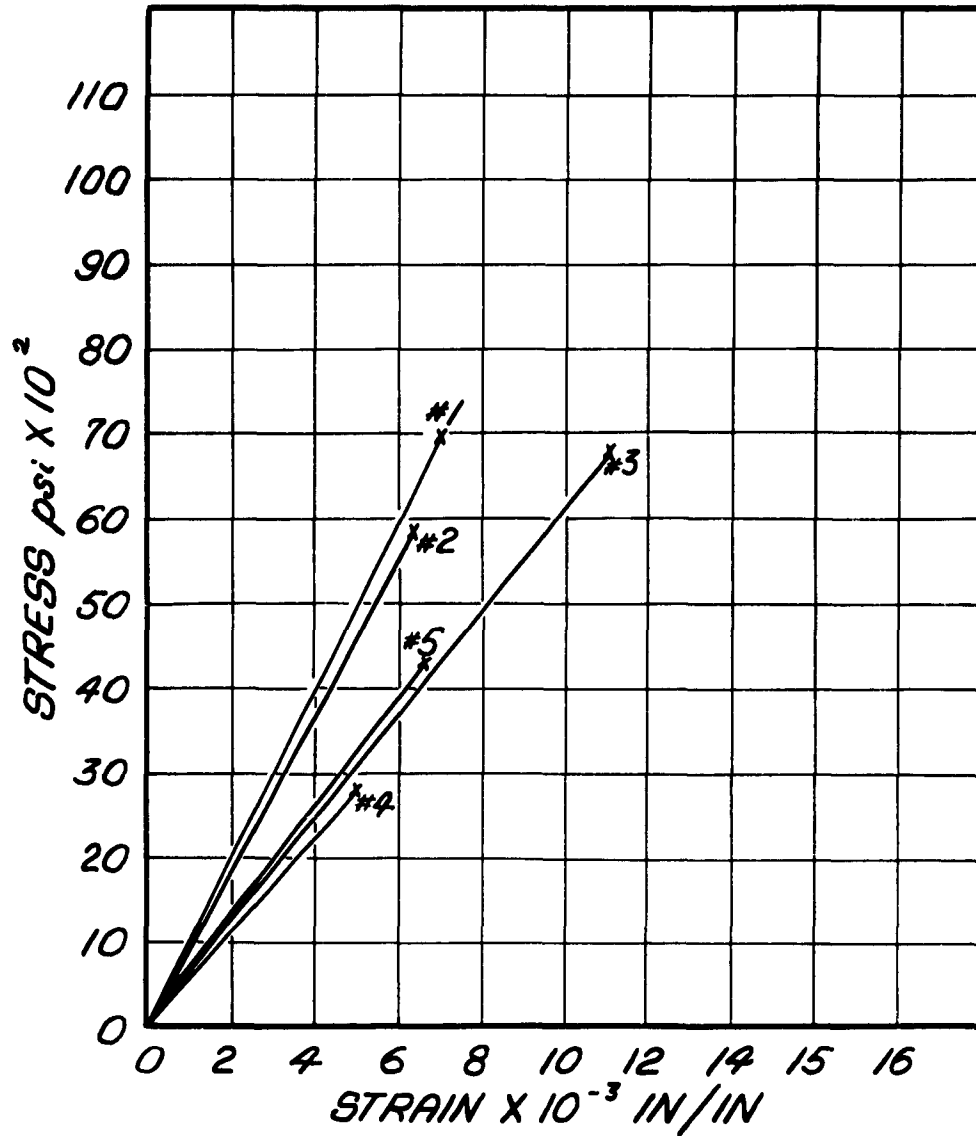


FIGURE 16

**STRESS-STRAIN CURVES FOR AMBLATE-
UNTREATED "N" GLASS COMPOSITE**

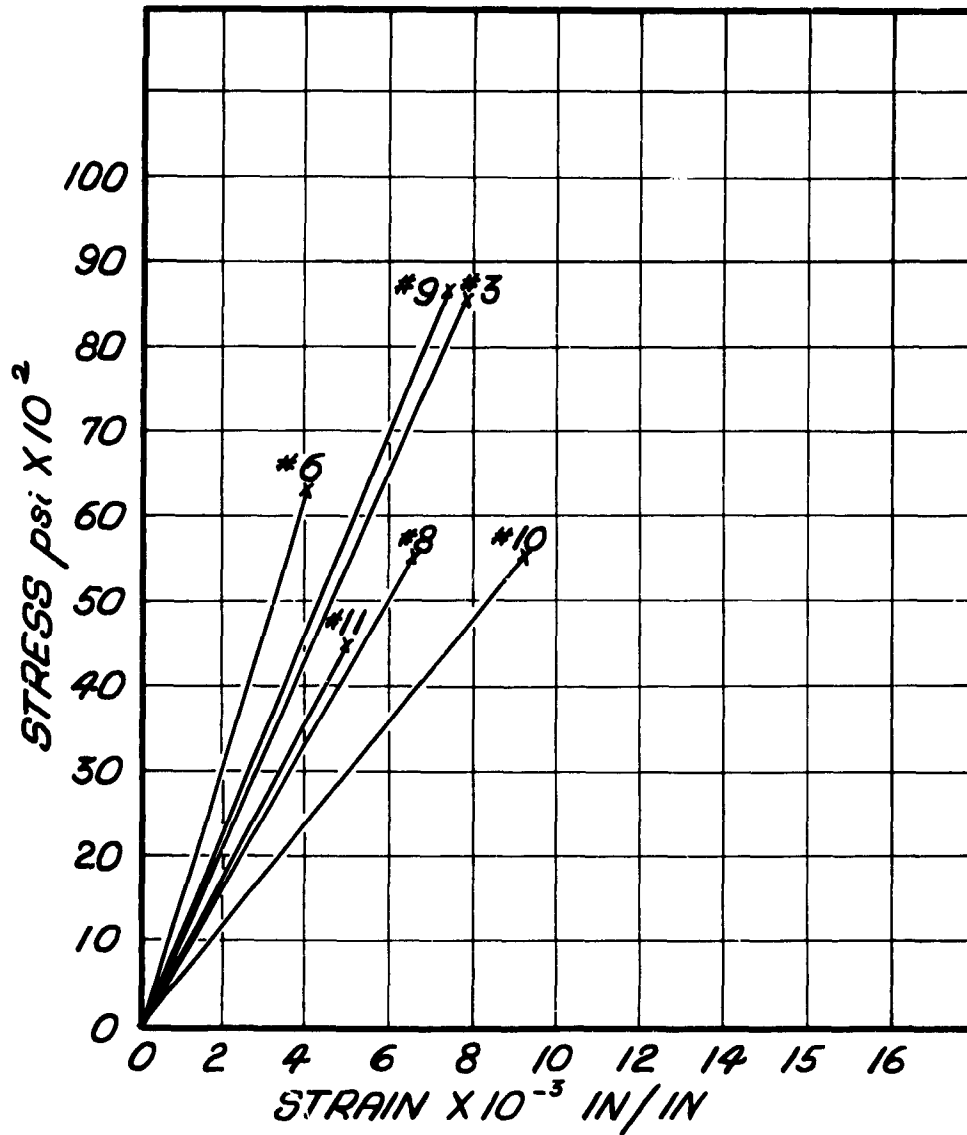


FIGURE 17

***STRESS-STRAIN CURVES FOR AMBLATE-
DESIZED 'N' GLASS COMPOSITE***

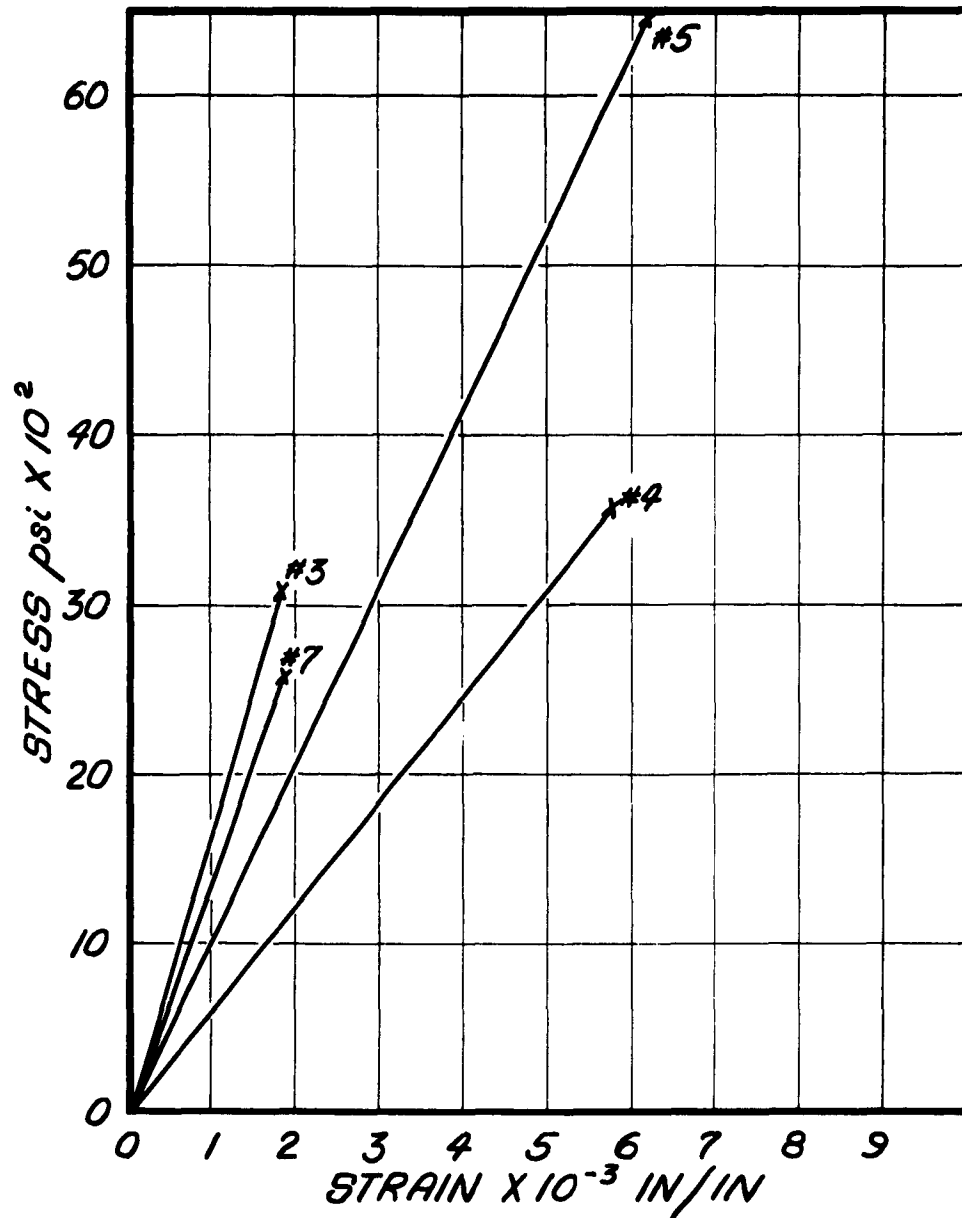


FIGURE 18

***STRESS-STRAIN CURVES FOR AMBLATE-
DESIZED 'N' GLASS COMPOSITE***

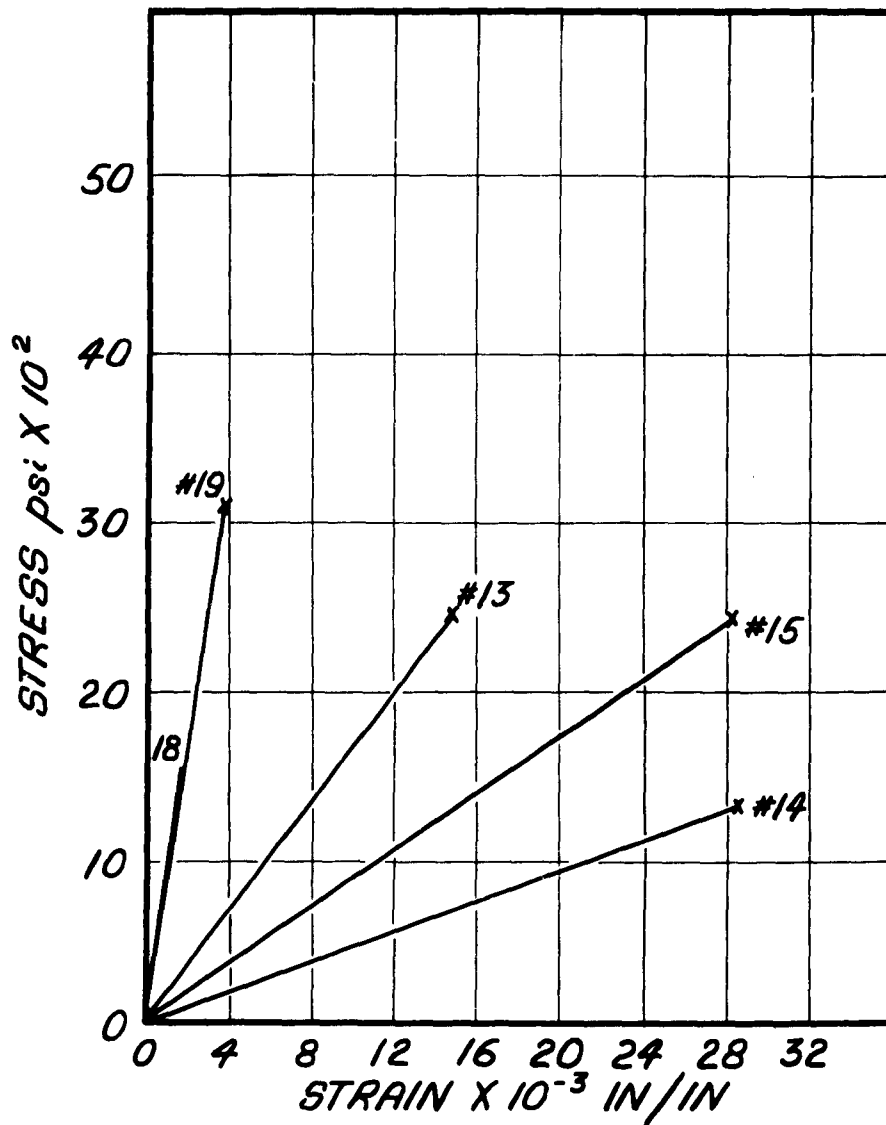


FIGURE 19



Figure 20. Amblate E- Glass Dry Pressed Composite.

B. LiF E-Glass Composite

A composite bar of E-glass fibers in a LiF matrix was prepared by the wet layup method. The bar was cut perpendicular to the fibers, the surface was carefully polished and examined using incident polarized, plane, and phase contrast illumination.

The LiF formed a rather porous matrix in places, as is shown in Figure 21. The glass fibers exhibited an inhomogenous distribution, forming congregations of many fibers and a random distribution of single fibers. The congregations were often associated with small voids in the bar, but the larger voids occurred where no fibers were present.

A marked difference was noted between the appearance of the single fibers and the appearance of the fibers in the center of the congregations. The single fibers appeared hazy and ill-defined, while the fibers in the center of the aggregates appeared the same as the isolated fibers. Closer inspection of this outside edge using incident phase contrast revealed that the fibers were fused together and were bordered by an apparent reactive ring. This is illustrated in Figures 22, 23, and 24. Slight fusion also occurred in the center fibers of the congregations, but not as severe as in the outer edge.

Since the glass fibers, by themselves, were unaffected by temperatures up to 1000° F, the LiF must act as a flux to reduce the fusion point of the glass. The isolated fibers and the outer fibers of the congregations had a greater contact with the LiF than the center fibers, hence a greater reaction occurred.

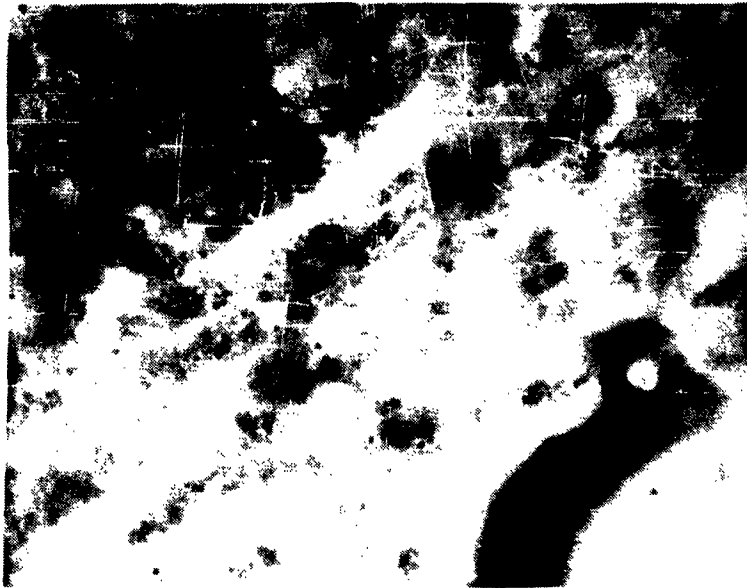


Figure 21. Porosity in LiF-Glass Fiber Composite Bar. Oblique Illumination X 100.



Figure 22. Inhomogenous Distribution of Glass Fibers in LiF-Glass Fiber Composite Bar. Incident Polarized X 100.



Figure 23. Fiber Congregation Showing Outer and Inner Portions. Incident Polarized Light X250.

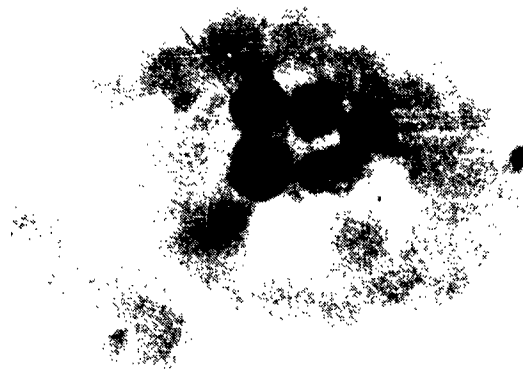
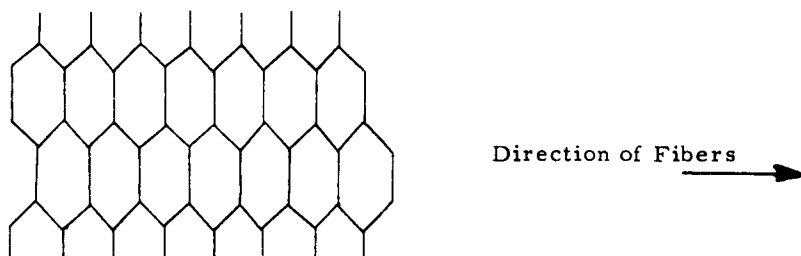


Figure 24. Fiber Congregation Showing Inner and Outer Portions and Outer Reaction Ring. Incident Phase Contrast. X 1050

In a search for a possible reinforcement to be used in the matrix E-18, boron fibers were tried. The fibers were manufactured by Texaco Experiment Incorporated, Richmond, Virginia, and the method of manufacture is described in their progress report TM-1278 (Ref. 2).

Untreated boron fibers of about .05 mm. diameter were observed under incident plain and polarized light and phase contrast illumination. The surface of the fibers show many distinct cells, highly resembling the grains on an ear of corn. The individual grains range in size from .0025 mm. to .012 to the length of the fiber. The arrangement seems to roughly resemble the diagram below:



Circular sections cut through the fibers and polished clearly show the tungsten substrates. Several dark radii were also observed in all of the circular sections. The radii ranged from four to two in number. The three radii are always 120° apart while the two radii are usually 180° apart. These radii appear to be planes of weakness or change, although relatively few fractures have been observed along these planes in untreated fibers. The radii met in the center of the tungsten wire and extended outward to the edge of the fiber.

The fibers are opaque and no optical properties could be obtained. Although no birefringence could be observed in any of the fibers, the cleavage denotes an internal atomic arrangement. The hexagonal-like arrangement of the surface features also suggests a crystalline substance. However, Texaco Experiment Incorporated in TM-1289 (Ref. 3) state that the fibers consist of a crystalline core surrounded with amorphous boron.

These boron fibers were then placed in a matrix of E-18 and fired for 100 hours at 1000°F . At the end of the 100 hours, the matrix sample was cut, polished, and observed with incident light. The fibers were clearly visible and seemingly unchanged. A slight reaction ring surrounded a few of the fibers, but nothing so severe as those obtained by using glass fibers.

The surface of the fibers show different degrees of reaction with the E-18, even over very small distances on the same fiber. The first stage is a light etch of the grains followed by a more severe second stage which darkened the grains and caused deeper pits. The third, and most severe

stage, is an obliteration of the grains and the formation of pin holes .001 to .002 mm. in depth. The reaction stopped at a definite time except in a few places where pin holes occurred. The etch attacked the grain boundaries most heavily, indicating a high energy level at the boundaries.

Cleavage was much more apparent in the E-18 surrounded fibers than in the untreated fibers. Again, the fibers cleaved along the planes of the radii parallel to the length of the fiber. These planes met at the center of the fibers and extended radially outward. Perfect cleavage perpendicular to the length of the fibers was also exhibited.

No change in the optical properties of the treated fibers could be noticed.

The fibers broke in several places when polishing was attempted while the fibers were still in the E-18. Portions of several of the fibers pulled loose and left their molds in the E-18, indicating a poor to fair matrix-fiber bond. It could not be determined if the fibers were more brittle after firing than before.

Although the surfaces of the fibers showed etching and cleavage increased, the boron fibers were still present after firing in E-18. This is a great improvement over glass fibers and cannot be overlooked. Several other trials should be made before any definite conclusions are stated.

A photomicrographic study of the fibers is shown in Figures 25 through 30.

Texaco rates boron fibers as having a break strength of 490,000 #/in² and a modulus = 55×10^6 #/in².

Figure 31 shows a boron fiber processed in an amble matrix. The fiber is in excellent condition, with some etching of the grain boundaries. This is very slight, however, and should not affect the strength to any great extent. Also, there is no reaction ring around the fiber which was present in the E-18 matrix specimens. It appears that the corrosion problem is much less severe with amble than with E-18 specimens.

A composite bar of boron fibers in an AlPO_4 LiF matrix that was fired at 1000°F was cut perpendicular to the length of the fibers. The surface was carefully polished and examined using incident polarized, plane, and phase contrast illumination.

Fibers in the amblygonite bars were seriously corroded. Pits and large cracks were present in all fibers as indicated in Figure 32. The spiral cleavage, previously mentioned, was greatly increased. The largest source of weakness, however, was the transverse cracks.

A composite bar of boron fibers in a LiF matrix that was fired at 1000°F was cut perpendicular to the length of the fibers. The surface was carefully polished and examined using incident polarized, plane, and phase contrast illumination.

Fibers in the LiF body were almost completely demolished as shown in Figure 33. It should be noted that a reaction ring surrounded the boron fiber in the composite body.

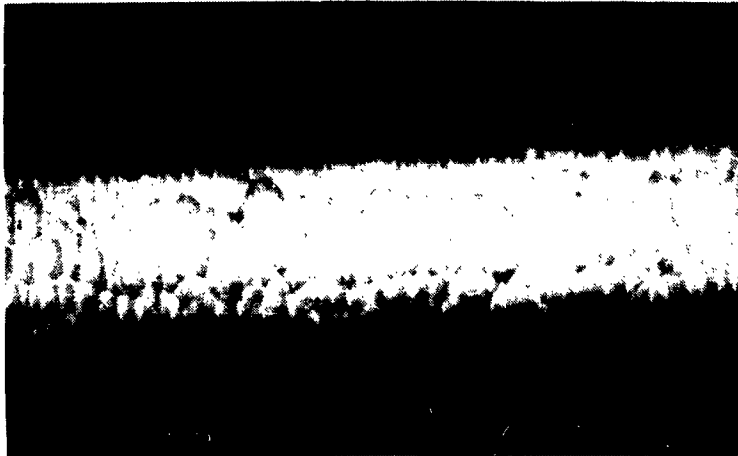


Figure 25. Boron Fiber Surface. X 1080



Figure 26. 1 mm Objective Micrometer Scale. X 1080



Figure 27. Boron Fiber(End View) in E-18 Matrix. X 1080

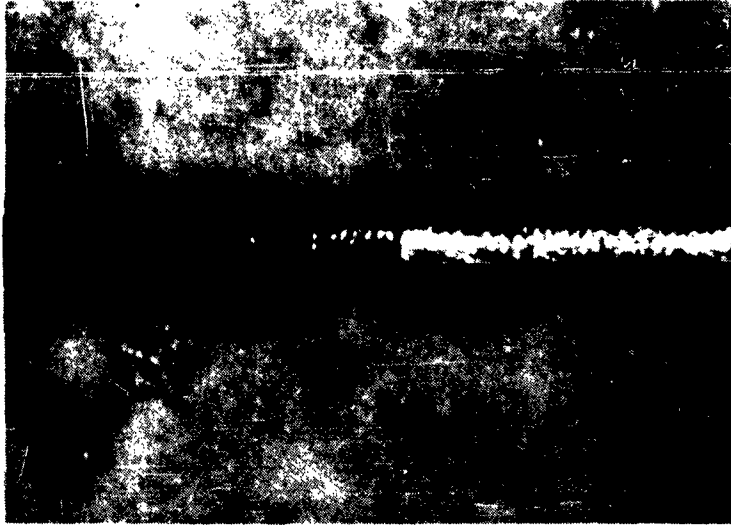


Figure 28 Boron Fibers in E-18. The Different Shades of the Fibers are caused by Different Stages in Etching. X240.



Figure29. Surface of Boron Fiber in E-18 Showing Etching Stages. X 1080.
 a. Initial etch of grains
 b. Darkening of grains and pitting
 c. Obliteration of grains and formation of pin holes



Figure 30. Normal view of a cleavage plane showing wire center (which is also cleaved), Heavily Etched Surface Profile, and Pin Holes Caused by Reaction With E-18. X 1080.

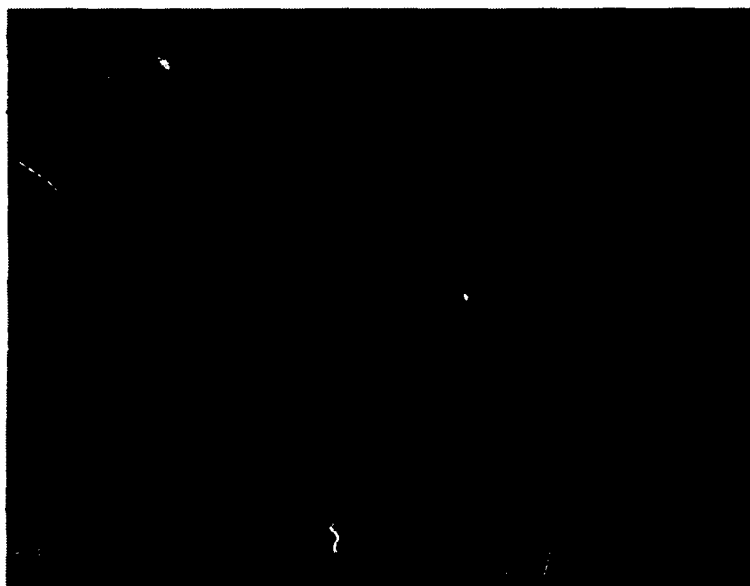


Figure 31. Amblate Matrix Boron Fiber. 60X



Figure 32. Boron Fiber After Being Fired in LiF Body.

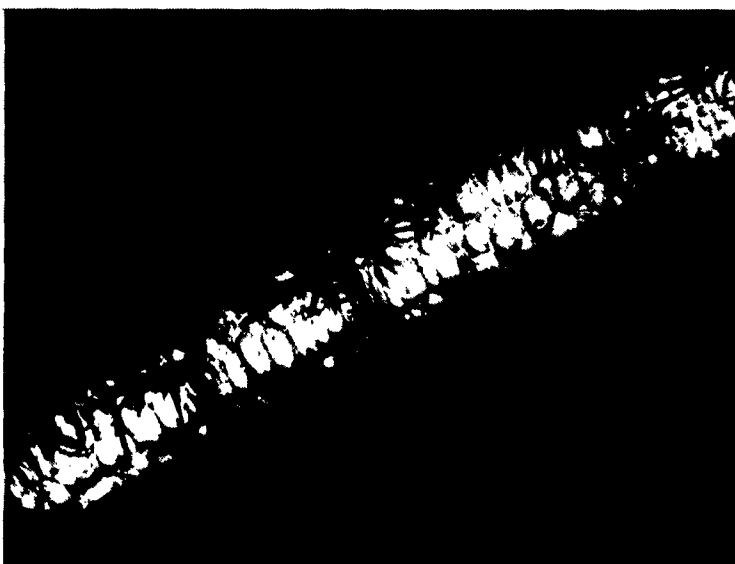


Figure 33. Boron Fiber After Being Fired in AlPO_4LiF Body.

IV. E-18 POLYMORPHIC STUDY

A. Detection and Identification of the Crystallographic Inversions Occurring in E-18 Oxide-Phosphate Bonded Specimens

As a result of precision measurements of the natural frequencies of vibration of oxide-phosphate bonded specimens, at temperatures from room temperature to 1200°C, some of the enantiotropic inversions of aluminum phosphate have been identified. Differential thermal analysis and X-ray diffraction methods were techniques also used to identify the same crystallographic inversions. The measurement of the effect of temperature on the total damping time is another method of determining the temperatures at which crystallographic inversions occur.

Figure 34 shows the effect of temperature on the modulus of elasticity of an oxide-phosphate bonded specimen. Five critical temperatures are noted, at which the modulus of elasticity begins to decrease. At three temperatures, 100, 800 and 960°C, there are peaks in the modulus curve. At two other temperatures, 210 and 550°C, there is a sudden decrease in the modulus. At temperatures above 1000 °C, the modulus is hard to measure by the dynamic method because of the increased damping at high temperatures.

The effect of temperature on the total damping of an oxide-phosphate bonded specimen is shown in Table 4. The damping procedure used is described in the appendix. Forster and Koster (Ref. 4) reported that the damping usually increases considerably during crystallographic transformation. The heat effects occurring in the E-18 oxide-phosphate material was also determined by means of differential thermal analysis. Five endothermic peaks were detected. The temperatures at which these heat effects occur are 224, 563, 954, 1006 and 1050°C. The results are tabulated in Table 5 along with the results of the damping and the dynamic modulus studies. An attempt was made to identify the inversions by comparing the characteristic temperatures with those reported by Beck (Ref. 5) for aluminum phosphate. The identification of the various crystallographic inversions are pretty reasonable, except for the inversions occurring at about 100 and 224°C. These inversions were identified as the α to β tridymite and the α to β cristobalite inversions. Normally, the tridymite and cristobalite forms of aluminum phosphate should not be present at these temperatures, but these phases could easily have been frozen in when the E-18 specimens were cooled quickly from the sintering temperature.

An X-ray diffraction study was initiated to help identify the crystallographic inversions occurring in the E-18 material. Samples were heated up to various temperatures and then quenched quickly in water. The temperatures used and the results of the X-ray diffraction studies of the specimens are shown in Table 6. It is apparent that there is an amorphous phase present in the samples which disappears at some temperature between 800 and 900°C. Beck states that the amorphous phase transforms over a range of temperatures, so it is possible that the amorphous to tridymite inversion has been depressed from 960°C to some temperature between 800°C and 900°C.

because the specimens were held at temperatures for at least one-half hour. In other words, when raising the temperature quickly from room temperature to 1000°C as in the differential thermal analysis and the damping time study, the fastest rate of transformation of the amorphous phase to tridymite occurs at 960°C. It also may occur at slower rates at lower temperatures.

Another phase was present in the specimens. This phase cannot be identified and has been given the name 'X'. It is probably a complex cobalt-aluminum phosphate because it transforms into $\text{Co}_3(\text{PO}_4)_2$ and possibly the cristobalite form of aluminum phosphate at some temperature between 980 and 1000°C.

It can be seen from the X-ray diffraction data that the crystallographic inversions occurring at 560°C and 800°C must be the α to β quartz and the quartz to tridymite inversions respectively. It may be possible that one of the two low temperature inversions might have been misnamed because according to the X-ray diffraction data, some of the amorphous phase changes to the quartz form of aluminum phosphate in that same temperature range.

B. X-ray Diffraction Studies of E-18 Oxide-Phosphate Bonded Material

X-ray diffraction techniques were used to determine the phases present in both the brittle and plastic E-18 matrix material specimens. In addition, X-ray diffraction patterns were taken of the as-reacted E-18 powder, and many other substances. The samples used are listed in Table 7. Identification was accomplished by comparing the X-ray diffraction patterns of the samples with the X-ray patterns of aluminum phosphate, alumina and other phases as found in the ASTM X-ray cards and as reported by investigators in the literature. The results are also tabulated in Table 7.

The E-18 as-reacted powder contained α alumina and an amorphous phase. Increasing the time of reaction didn't change the number nor the identity of the phases present, but more of the alumina had a chance to react with the phosphoric acid to form the amorphous phase.

When only aluminum oxide was reacted with phosphoric acid, there was some evidence of the quartz form of aluminum phosphate being present in the powder in addition to the amorphous phase. A number of different powders were prepared in which various amounts of cobalt oxide were added to the aluminum oxide before reacting the oxides with phosphoric acid. Analysis of the resultant powders revealed the presence of the quartz form of aluminum phosphate in every case, plus the amorphous phase in some cases. The addition of zinc oxide to the aluminum oxide resulted in α alumina and the quartz form of aluminum phosphate. When cobalt oxide alone was reacted with phosphoric acid, an amorphous phase resulted. Aluminum phosphate powder supplied by Fisher Scientific Co. had an amorphous structure.

X-ray diffraction patterns of the sintered E-18 material in test specimens which had been proven to be brittle, and others that had plastically deformed, indicate that the following phases are present:

Brittle

1. α Alumina
2. Cristobalite form of AlPO_4
3. Unidentified Phase X
4. Quartz form of AlPO_4
5. What appears to be an amorphous phase

Plastic

1. α Alumina
2. Cristobalite form of AlPO_4
3. Unidentified Phase X

So the brittle specimens contain two more phases than the plastic specimens. All of the diffraction patterns of both types of specimens contained a strong line ($d = 2.99\text{\AA}$) which hasn't been identified. It is possible that it indicates the presence of a cobalt phosphate phase or a more complex aluminum-cobalt phosphate phase. X-ray diffraction patterns of sintered bars prepared from pure alumina, which was reacted with phosphoric acid in the same manner as the E-18 mix was, showed the presence of α alumina, the quartz, and the cristobalite forms of aluminum phosphate, and no diffraction line at $d = 2.99\text{\AA}$. Typical data from the X-ray patterns are shown in Tables VIII, IX, and X.

The X-ray diffraction patterns of the brittle and ductile specimens indicate that the cristobalite form of aluminum phosphate was present in both types of specimens. This is interesting, because according to the crystallographic inversion temperatures found by Beck (Ref. 5) and by the authors of this report, there should not be any cristobalite present in any of the specimens.

One possible mechanism is the one reported by Shafer and Roy (Ref. 6). They reported that the quartz form inverts first to cristobalite and then the unstable cristobalite inverts to tridymite. This is analogous to a normal Oswalt stepwise mechanism. They also reported the quartz to tridymite inversion is at 707°C instead of at 815°C as reported by Beck. Using this information, the following explanation for the presence of cristobalite in the sintered E-18 specimens can be formulated.

If the presence of cobalt ions results in a depression of the quartz form to cristobalite form inversion from 707°C to some temperature below 650°C , then the tridymite form of aluminum phosphate will be the stable state at 650°C . Thus as the bar is sintered at 650°C for four hours, the quartz form inverts first to cristobalite and subsequently to tridymite. When the specimens are removed from the furnace they cool quickly to about $100\text{--}200^\circ\text{C}$. The tridymite probably quickly transforms to cristobalite, which is reasonable, since they only differ in stacking sequence in one dimension. The cristobalite does not have a chance to invert to the quartz form because it is more a difficult reconstructive transition.

A possible reason for the difference in physical properties of the sintered E-18 specimens is that all of the quartz and amorphous phases must be transformed to tridymite at elevated temperatures before the specimen will plastically deform.

If the cobalt ions cause a depression of the quartz to tridymite inversion temperature, then the peak identified in Table V at 800°C as the quartz to tridymite inversion point is in error. Of course, sintering at 650°C may cause depression of the inversion point, while it is at a higher temperature when the material is continuously heated.

V. EQUIPMENT

A. Automatic Stress-Strain

To determine the modulus of rupture and the deformation behavior of composite specimens, a new automatic system of stress-strain recording has been developed (Figure 35). The load information fed to the x-y recorder is obtained by mounting an SR-4 strain gauge on a plastic strip which links the loading bucket with the balancing bridge circuit as shown in Figure 36. A compensating SR-4 strain gauge is also connected into the bridge circuit, so that any changes in resistance of the load strain gauge due to a change in temperature is balanced by a similar change in the compensating strain gauge. The bridge circuit includes two variable resistors which are used to zero the output of the bridge circuit when no load has been applied to the test specimens. This is equivalent to saying that the resistors are adjusted until the y axis reads zero on the x-y recorder when no load has been applied. A twelve volt lead battery was used as an external potential source for the bridge circuit. Thus, the balancing bridge circuit transforms the changes in resistance of the strain gauge into potential differences which drive the y axis of the function plotter.

The deflection was measured by means of a recrystallized quartz rod which rests on top of the loading yoke (which includes the loading knife edge.) The quartz rod extends up through a hole in the roof of the furnace and also through a hole in a plastic U-shaped fixture. The other end of the rod rests against a thin strip of stainless steel which is held in place by the plastic U-shaped fixture. An SR-4 strain gauge was mounted on the stainless steel strip to supply strain information to the x-y function plotter.

Before any load is applied to the test specimen, the quartz bar is high enough to cause the stainless steel strip to be flexed. As the load is applied, the test specimen deflects, causing the loading edge and yoke to drop down. This, in turn, causes the free riding quartz rod to drop with a resultant unflexing of the stainless steel strip, which, in turn, is measured by SR-4 strain gauge.

The strain gauge is connected to a Baldwin-Lima-Hamilton Type N strain indicator which has been modified to act as a bridge circuit which converts the strain gauge resistance variations into variations of electrical potential which are in effect amplified by the other circuits in the strain indicator. The resultant electrical potential is fed to the x axis of the function plotter.

**MODULUS OF ELASTICITY VS. TEMPERATURE
PHOSPHATE BONDED OXIDE BODY**

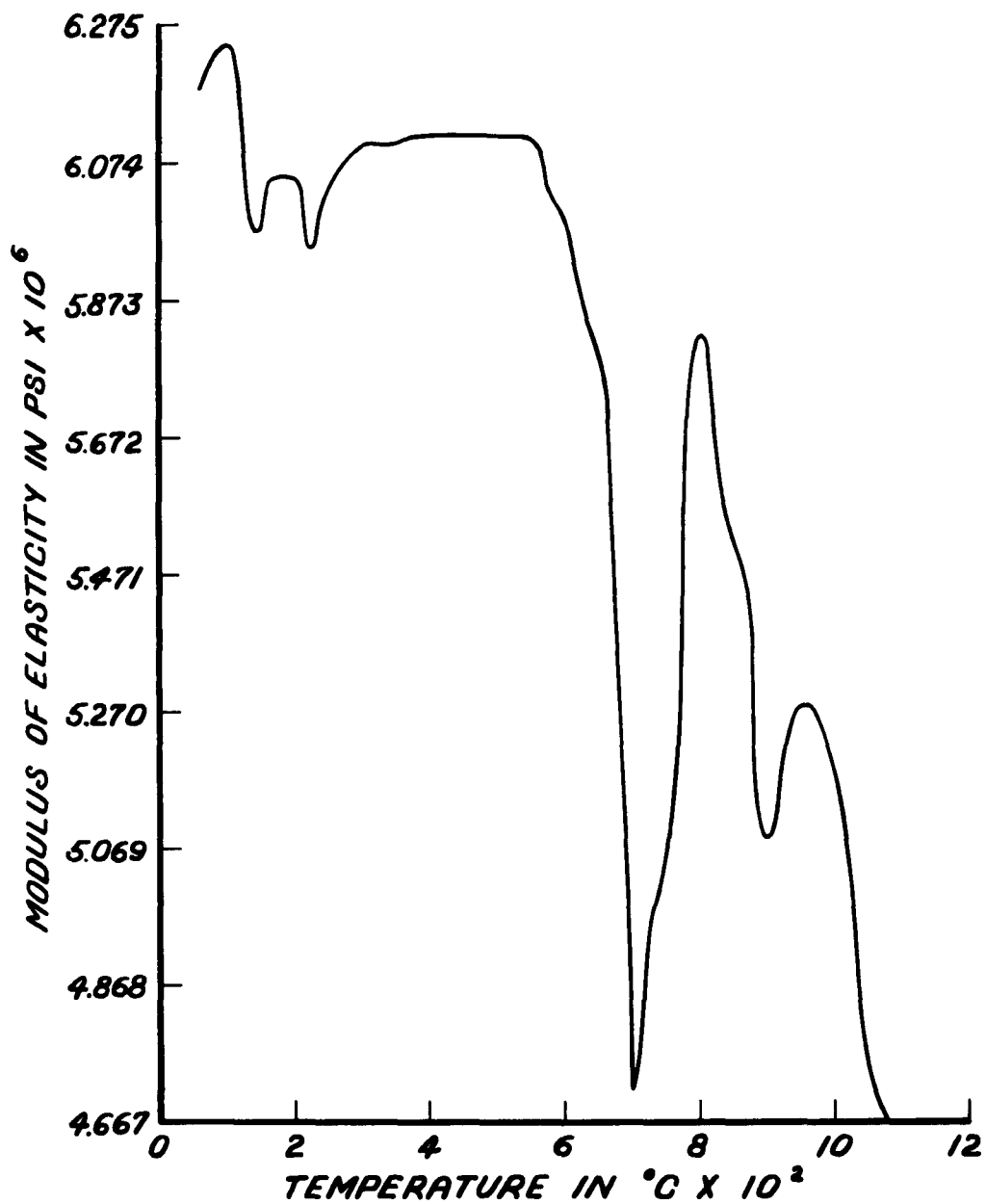


FIGURE 34

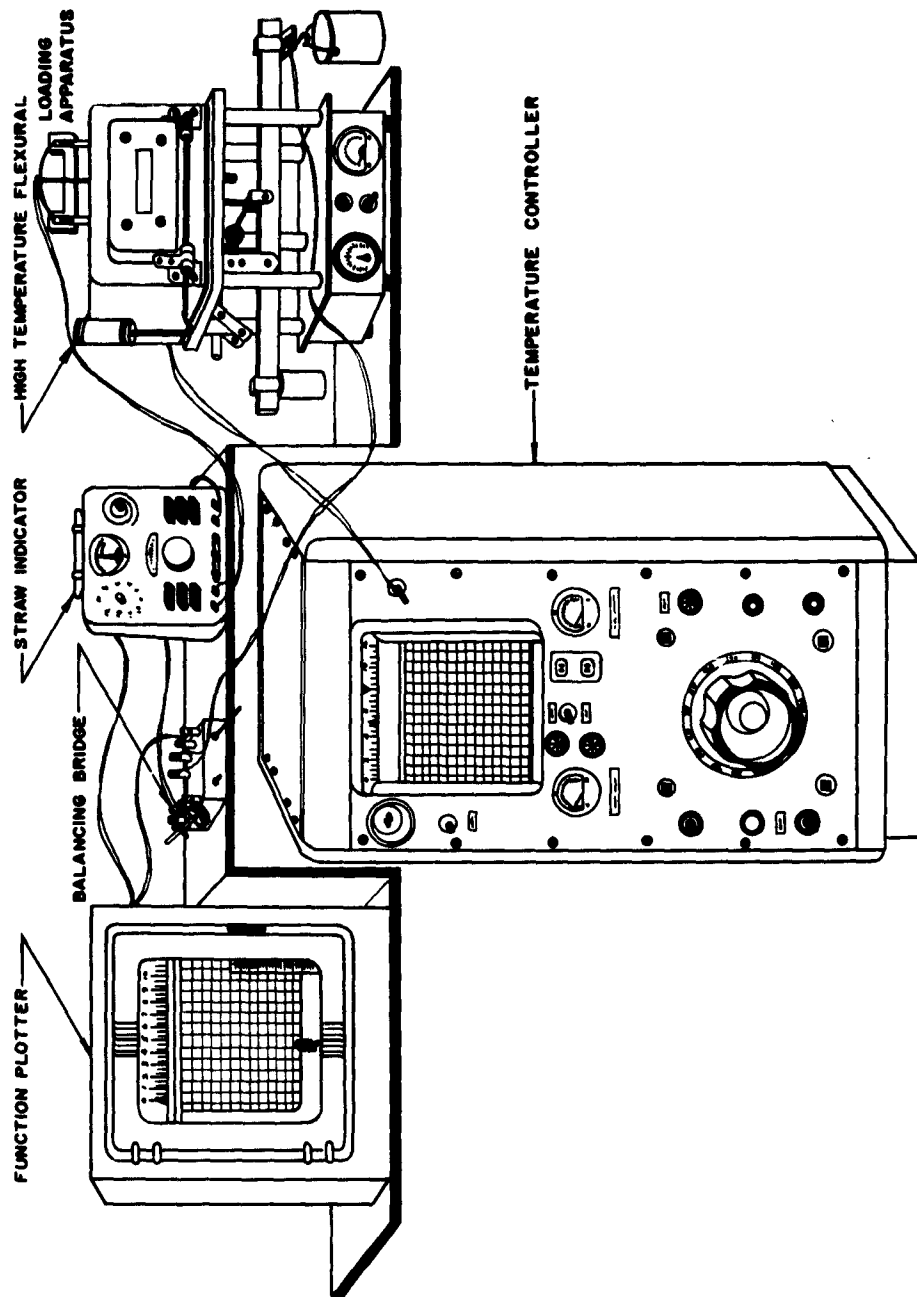
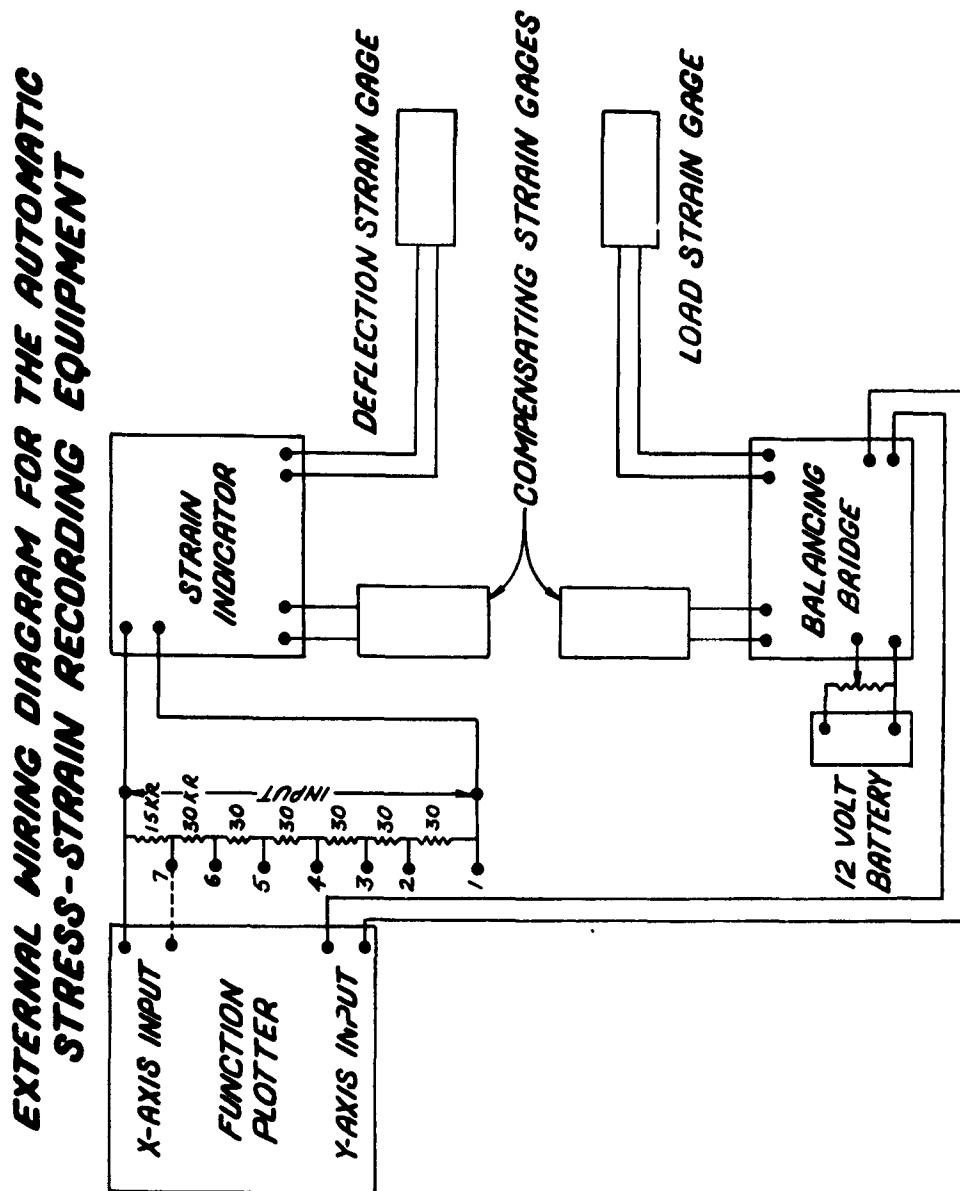


FIGURE 35

AUTOMATIC STRESS - STRAIN RECORDING EQUIPMENT

FIGURE 36



Before the equipment can be used to automatically measure the load and the deflection, the x and y scales of the function plotter have to be calibrated. For example, the scale reading on the y axis was recorded when known loads were added to the loading bucket. The load is plotted versus scale readings in Figure 37 for both the 5 volt and the 10 volt scale.

To calibrate the y axis of the function plotter, a bar was flexed, and the scale reading was recorded along with the corresponding amount of deflection. The deflection was determined by measuring the movement of a mark on the quartz rod with a micrometer eyepiece. The deflection is plotted versus scale readings in Figure 38. There are seven curves, each curve represents a different amount of input to the function plotter (compared to output of strain indicator. This is accomplished by connecting the function plotter input lead to the different contact points of the resistance network (as seen in Figure 36.)

To determine the physical properties of a composite specimen the following procedure was used:

1. A rectangular specimen (6" X 1" X 3/16") was placed in the furnace and allowed thirty minutes to reach temperature equilibrium.
2. The specimen was then mounted on the supporting knife edges and the loading knife edge was placed on the bar.
3. The x and y coordinates of the function plotter were zeroed by means of the variable resistors in the balancing bridge circuit and the strain indicator.
4. The load was applied at a uniform rate of 1.5 pounds per minute.

A typical result is shown in Figure 39. This is a stress-strain curve for an E-18 oxide-phosphate bonded specimen sintered at 650°C for four hours after the powder was reacted at 300°C for five hours.

***CALIBRATION CURVES FOR THE X-AXIS
OF THE FUNCTION PLOTTER***

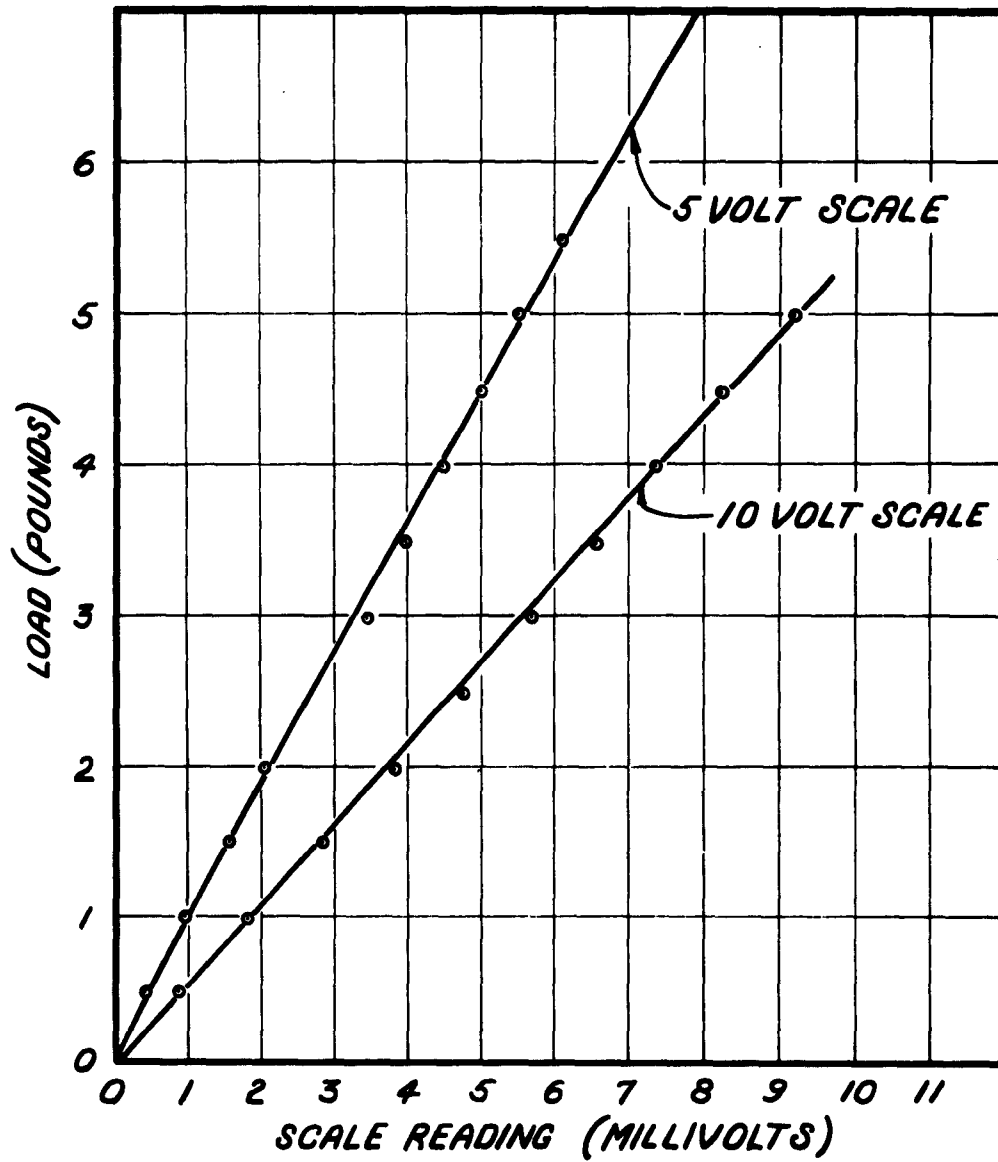
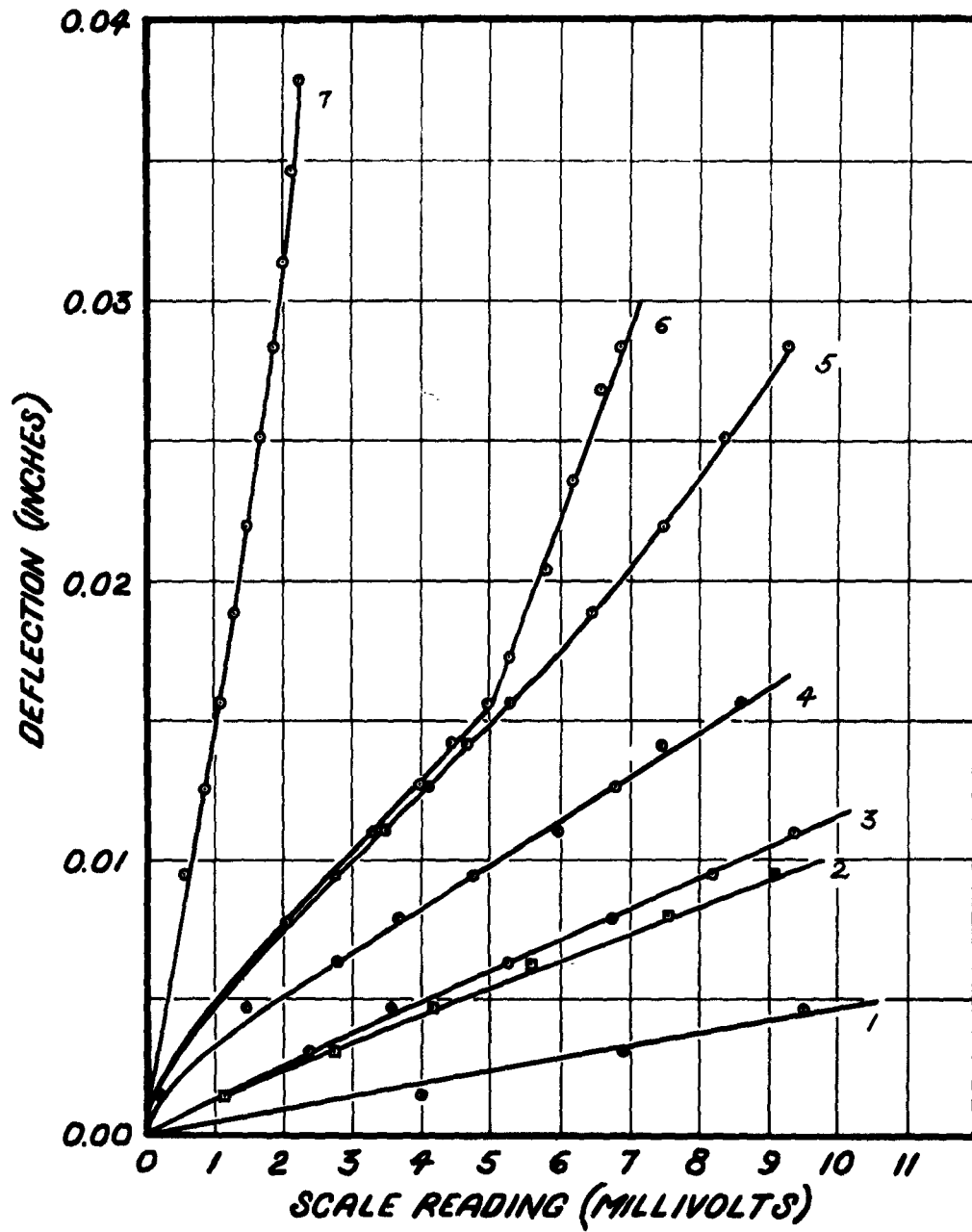
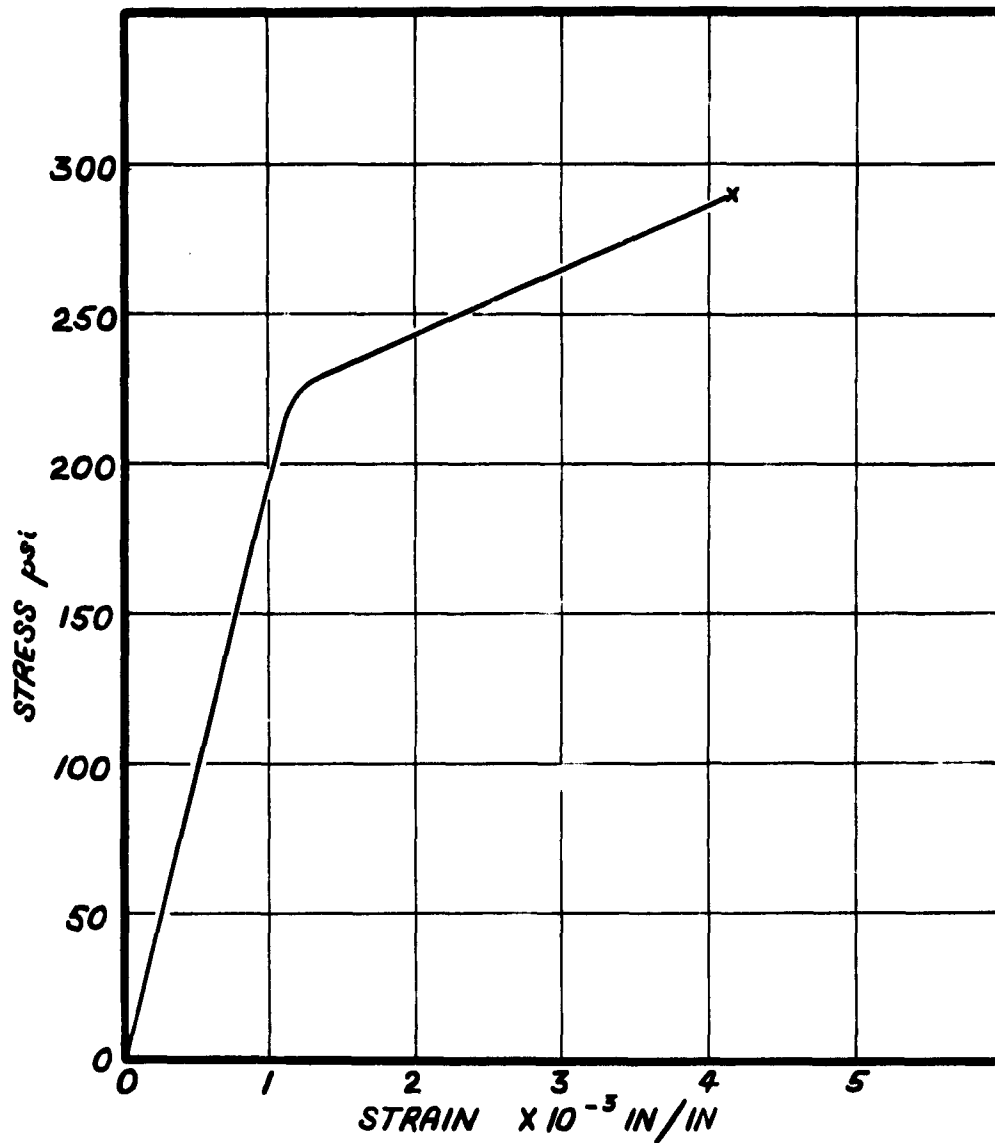


FIGURE 37

FIGURE 38

***CALIBRATION CURVES FOR THE Y-AXIS
OF THE FUNCTION PLOTTER***





**ENGINEERING STRESS-STRAIN CURVE
FOR SAMPLE 5B**

FIGURE 39

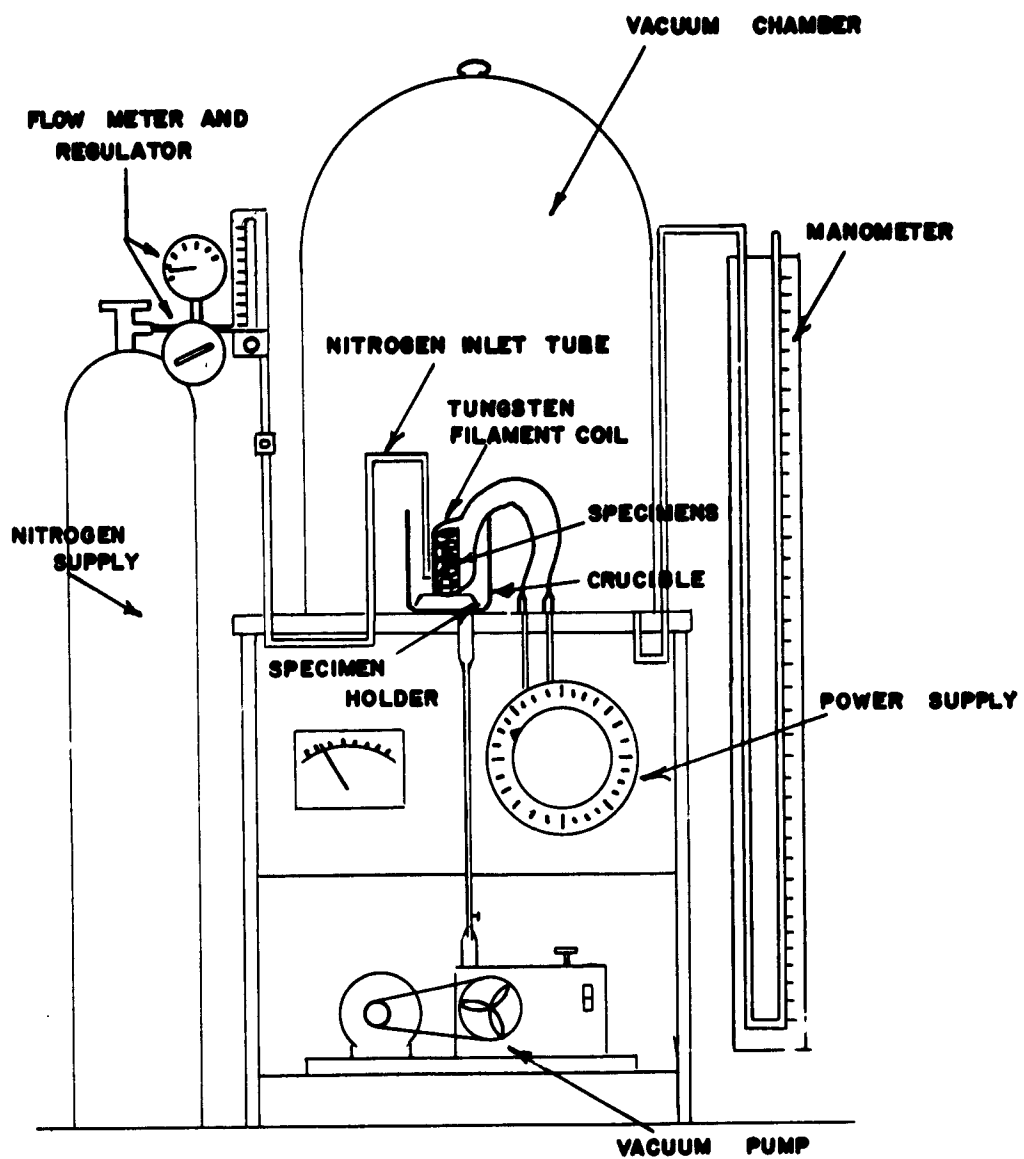
B. Nitriding System

A type of experimental nitriding system was designed to determine experimentally if it was feasible to produce a boron nitride film on the surface of boron fibers or filaments. The investigation was conducted by the systematic manipulation of the following variables: specimen temperature, nitrogen flow rate, and time.

This investigation was performed on the basis that boron nitride being an inert basic material will afford a satisfactory protective film on the surface of the boron fibers.

The nitriding system was made up of the following component parts:
(See Figure 40).

1. Mechanical vacuum pump-- to maintain a partial pressure.
2. Base Plate and bell jar for working area.
3. Manometer to measure partial vacuum.
4. Tungsten wound coil surrounding specimen holder to supply a specimen temperature of 1000-5000°F.
5. Fiber specimen holder which will enable the boron fibers to be mounted vertically inside the tungsten filament coil.
6. Ceramic insulator sleeve to prevent excess radiation and also make it possible to maintain a more constant temperature.
7. Nitrogen supply and inlet tube. Also flow meter to meter in required amount of nitrogen directly to hot zone where it may be dissociated and reacted on the hot surface of the boron fibers to form a boron nitride film.
8. Optical pyrometer to measure temperature of the hot zone.



NITRIDING SYSTEM

FIGURE 40

VI. DISCUSSION OF RESULTS

The strength of the composites using amblate as the binder, as shown in Figures 10 through 19, varies quite a bit between lots. Lot being defined as a group of specimens prepared with the reinforcement fibers receiving the same pretreatment. The specimens prepared with untreated E-glass reinforcement fibers had modulus of rupture strengths varying between 1000 psi and 7000 psi with the average being about 4000 psi. This was the modulus of rupture value for the amblate matrix without reinforcement. In addition, the strain varied between 3×10^{-3} in./in. and 8×10^{-3} in./in. The specimens prepared from these fibers, untreated E-glass, did not have reproducible properties.

The next lot of composites prepared from desized E-glass proved to have good strength and reproducibility. Modulus of rupture values ranged from 7000 psi to above 11,000 psi, with an average of about 9000 psi. This strength is over double that of the amblate matrix alone, which is very remarkable considering the amount of fibers added to the matrix was less than five per cent. Strain values ranged from 3×10^{-3} in./in. to 4×10^{-3} in./in. Very good reproducibility was obtained in stress values.

The composites formed with untreated "N" glass reinforcement fibers had fairly good reproducibility, but, in general, poor strength. Modulus of rupture values were in the range of 5000 psi and the strain value in the range of 7×10^{-3} in./in. This strength value is just above the strength value obtained for the unreinforced amblate matrix.

The composites of amblate reinforced with desized "N" glass fibers had lower strength and less reproducibility than specimens made from the untreated fibers. This lower value was most likely due to the deterioration of the fibers during the desizing operation. This would also explain the wide variance in these values.

The effort spent during the project on corrosion protection was necessary. However, once the corrosion problem was alleviated, the project was then faced with the basic problem of how to transfer the load from the matrix to the fibers. There have been several studies made on this same mechanism in the organic matrix system, (Ref. 7, 8) but no definite conclusions were made. The theory that seemed to fit experimental data best was that the coefficient of friction between the matrix and the fiber was high enough to prevent any movement between the fiber and matrix.

In general, the potential types of composite bonding are few. These types of bonding are chemical, mechanical or a combination of the two. Chemical bonding to a glass with any degree of strength would be very difficult. The bonding would be restricted to ionic or covalent bonding of a superficial surface layer.

Mechanical bonding would be preferable, if it could be accomplished without destroying the surface perfection of the fibers. This again would be very difficult

to accomplish as the grains in the ceramic matrix are very hard and sharp. During the processing, especially the dry pressing, it is conceivable that many hundreds of the grains fracture the surface of the fibers. In addition, the amount of mutual surface area of the matrix and the fibers would be small. An idea of the available contact area could be visualized by stacking BB's around a pencil and noting the mutual surface areas.

It would be profitable if a research study could be made on the different ways to bond the matrix to the reinforcement fibers and the feasibility of such methods.

Another unsolved problem was how to obtain a homogenous mixture of fibers in the matrix in dry pressed composites. The method utilized in this project was very poor as about five per cent fibers was the maximum addition of fibers. It is possible that this problem, if considered by personnel outside the materials area, could be solved.

The boron fiber study indicated that the fibers had potential. The brittleness of the fibers and time considerations precluded the fibers from receiving a thorough study.

The polymorphism study of AlPO_4 revealed some interesting data, and in addition, revealed a problem that was too large in magnitude for the effort available. It is felt however, that the inelastic deformation tendencies of AlPO_4 is connected directly to this polymorphism.

An apparatus was designed and constructed for nitriding boron fibers. Specimens which were treated to the nitriding process were examined by electron microscope and optical techniques which revealed that the process was feasible,

VII. CONCLUSIONS

Fiber reinforced inorganic matrix composites are feasible. An inorganic matrix composite, reinforced with five per cent fibers, had a modulus of rupture two and one-half times that of the matrix alone. A method to increase the total amount of fibers in the composite would undoubtedly increase the strength much above two and one-half times.

The method of bonding fibers in the composite is restricted to a mechanical, frictional type at present. Fundamental studies on this problem could lead to a composite with much higher strength.

The unreproducibility of the E-18 matrix material is connected to the polymorphism of the AlPO_4 . X-ray and differential thermal analysis of the E-18 reveals different compositions of supposedly same material.

Boron fibers have a higher degree of corrosion resistance than glass fibers. These fibers, however, are much more brittle which presents fabrication problems.

VIII. REFERENCES

1. J. H. Lauchner, W. B. Hall, and J. M. Fields, Jr., "High Temperature Inorganic Structural Composite Materials," (Final Report) Mississippi State University, Aeronautical Systems Division Technical Report, 62-202, Part I, November, 1962.
2. Claude P. Talley, Wendall J. Clark, and Franklin E. Wawner, Jr., "New and Improved Reinforcements for Structural Composites," Texaco Experiment Incorporated, TM-1278, Quarterly Progress Report for 15 March - 15 June, 1961.
3. Claude P. Talley, Wendall J. Clark, and Franklin E. Wawner, Jr., "New and Improved Reinforcements for Structural Composites," Texaco Experiment Incorporated, TM-1289, Quarterly Progress Report for 15 June - 15 September, 1961.
4. F. Forster and W. Koster, "Elasticity and Damping in Relation to the State of the Materials," Engineer, 166, 626, (1938).
5. W. R. Beck, "Crystallographic Inversions of the Aluminum Orthophosphate Polymorphs and Their Relation to those of Silica," J. Am. Cer. Soc., 32, 147, (1949).
6. E. C. Shafer and R. Roy, "Studies of Silica Structure Phases, III: New Data on the System AlPO_4 ," Zeitschrift fur Physikalische Chemie, 11-12, 30, (1957).
7. J. S. Islinger, K. Gutfreund, R. G. Maguire, O. H. Olson, "Mechanism of Reinforcement of Fiber Reinforced Structural Plastics and Composites," (Final Report) Armour Research Foundation, Wright Air Development Division Technical Report 59-600, Part I, March, 1960.
8. Yehuda Stavsky, Frederick J. McGarry, "Investigation of Mechanics of Reinforced Plastics," Massachusetts Institute of Technology, Wright Air Development Division Technical Report 60-746, October, 1959.

TABLE I. EXPERIMENTAL MATRIX COMPOSITION

Specimen	Al_2O_3 gms	AlPO_4LiF gms	Co_3O_4 gms.	ZnO gms	H_2O cc	H_3PO_4
1	200	500	50	5	200	125
2	200	500	50	5	200	200
3	300	400	75	10	200	125
4	300	400	75	10	200	175
5	300	400	50	5	200	125
6	300	400	50	5	200	175

TABLE II. PROPERTIES OF AMBLATE MATRIX

Specimen	Modulus of Rupture psi	Deflection in/in
1	2406	.010
2	2637	.032
3	4163	.022
4	3738	.037

TABLE III. MODULUS OF ELASTICITY OF
CaF₂ AND AlPO₄LiF

Specimen	Sintering Temperature Degrees F	Room Temperature Degrees F	E x 10 ⁶
F1	1800°F	room temperature	.5917
		1000°	.6261
F2	1600°F	room temperature	.4035
		1000°	.4286
F3	1600°F	room temperature	.7634
		1000°	.8729
F4	1600°F	room temperature	.5091
		1000°	.5344
F5	1800°F	room temperature	.8937
		1000°	.9191
F6	1800°F	room temperature	1.1924
		1000°	1.1981
F7	1800°F	room temperature	.6963
		1000°	.7221
F8	1800°F	room temperature	1.2006
		1000°	1.2416
A1	1400°F	room temperature	1.4762
		1000°	1.3583
A2	1400°F	room temperature	1.3250
		1000°	1.2326
A3	1400°F	room temperature	1.3911
		1000°	1.3589
A4	1400°F	room temperature	1.2405
		1000°	1.1755
A5	1400°F	room temperature	1.8685
		1000°	1.6571
A6	1400°F	room temperature	3.2984
		1000°	3.4541
A7	1400°F	room temperature	2.6887
		1000°	2.4081
A8	1400°F	room temperature	2.5996
		1000°	2.4154
A9	1400°F	room temperature	1.6623
		1000°	1.9036
A10	1450°F	room temperature	.9491
		1000°	.8740
A11	1450°F	room temperature	2.0629
		1000°	2.2413
A12	1400°F	room temperature	1.7895
		1000°	2.0750
A13	1400°F	room temperature	2.7054
		1000°	2.4715
A14	1400°F	room temperature	1.7337
		1000°	

TABLE IV. EFFECT OF TEMPERATURE ON THE TOTAL DAMPING TIME
OF AN OXIDE-PHOSPHATE BONDED SPECIMEN

Temperature	Total Damping Time (seconds)	Temperature (°C)	Total Damping Time (seconds)
60	0.091	480	0.059
80	0.093	500	0.053
100	0.095	520	0.045
120	0.101	540	0.043
140	0.073	560	0.049
160	0.074	580	0.041
180	0.075	600	0.041
200	0.078	620	0.041
220	0.089	640	0.041
240	0.086	660	0.041
260	0.085	680	0.041
280	0.081	700	0.041
300	0.080	720	0.041
320	0.077	740	0.041
340	0.076	760	0.041
360	0.074	780	0.041
380	0.068	800	0.041
400	0.061	820	0.041
420	0.066	840	0.041
440	0.065	860	0.040
460	0.063	880	0.040

TABLE IV. EFFECT OF TEMPERATURE ON THE TOTAL DAMPING TIME
OF AN OXIDE-PHOSPHATE BONDED SPECIMEN, CONT'D.

Temperature (°C)	Total Damping Time (seconds)	Temperature (°C)	Total Damping Time (seconds)
900	0.040	1020	0.036
920	0.036	1040	0.038
940	0.037	1060	0.032
960	0.039	1080	0.036
980	0.037	1100	No
1000	0.038		

TABLE V. DETECTION AND EVALUATION OF CRYSTALLOGRAPHIC INVERSIONS
IN E-18 OXIDE-PHOSPHATE BONDED SPECIMENS

Differential Thermal Analysis Effect of Temperature on Modulus of Elasticity Effect of Temperature on Damping Time								
Temp. °C	Effect	Inversion	Temp. °C	Effect	Inversion	Temp. °C	Effect	Inversion
224	Endothermic Peak	$\alpha \rightarrow \beta$ Cristobalite	100	Peak	$\alpha \rightarrow \beta$ tridymite	120	Peak	$\alpha \rightarrow \beta$ Tridymite
563	Endothermic Peak	$\alpha \rightarrow \beta$ Quartz and amorphous to quartz	210	Beginning of sudden decrease in modulus	$\alpha \rightarrow \beta$ cristobalite	220	Peak	$\alpha \rightarrow \beta$ Cristobalite
			550	Beginning of sudden decrease in modulus	$\alpha \rightarrow \beta$ Quartz and amorphous to quartz	560	Peak	$\alpha \rightarrow \beta$ Quartz and amorphous to quartz
954	Endothermic Peak	Amorphous to tridymite	800	Peak	Quartz to tridymite	960	Peak	Amorphous to tridymite
1006	Endothermic Peak	Amorphous to cristobalite		Peak	Amorphous to tridymite	1000	Peak	Amorphous to cristobalite
1050	Endothermic Peak	Tridymite to cristobalite				1040	Peak	Tridymite to cristobalite

TABLE VI. PHASES PRESENT IN E-18 OXIDE-PHOSPHATE BONDED SPECIMENS QUENCHED FROM VARIOUS TEMPERATURES

Specimen	Temperature (°C)	Phases Present
22	140	α -Al ₂ O ₃ + Amorphous Phase + Phase X
23	240	α -Al ₂ O ₃ + Amorphous Phase + Phase X + Quartz
24	300	α -Al ₂ O ₃ + Amorphous Phase + Phase X + Quartz
25	400	α -Al ₂ O ₃ + Amorphous Phase + Phase X + Quartz
27	540	α -Al ₂ O ₃ + Amorphous Phase + Phase X + Quartz
28	600	α -Al ₂ O ₃ + Amorphous Phase + Phase X + High Quartz
29	660	α -Al ₂ O ₃ + Amorphous Phase + Phase X + High Quartz
30	680	α -Al ₂ O ₃ + Amorphous Phase + Phase X + High Quartz
31	700	α -Al ₂ O ₃ + Amorphous Phase + Phase X + High Quartz
32	720	α -Al ₂ O ₃ + Amorphous Phase + Phase X + High Quartz
33	800	α -Al ₂ O ₃ + Amorphous Phase + Phase X + High Quartz
34	900	α -Al ₂ O ₃ + Phase X + Tridymite
35	980	α -Al ₂ O ₃ + Phase X + Tridymite + Cristobalite
36	1000	α -Al ₂ O ₃ + Co ₃ (PO ₄) ₂ + Cristobalite

TABLE VII. RESULTS OF X-RAY DIFFRACTION STUDIES

Specimen No.	Specimen	Phases Present in the Specimen
2	E-18 As-sintered--Brittle	α Al_2O_3 + Cristobalite + Quartz + Phase X + Amorphous Phase
4	E-18 As-sintered--Brittle	α Al_2O_3 + Cristobalite + Quartz + Phase X + Amorphous Phase
5	E-18 As-sintered--Brittle	α Al_2O_3 + Cristobalite + Quartz + Phase X + Amorphous Phase
6	E-18 As-sintered--Brittle	α Al_2O_3 + Cristobalite + Quartz + Phase X + Amorphous Phase
1	E-18 As-sintered--Plastic	α Al_2O_3 + Cristobalite + Phase X
3	E-18 As-sintered--Plastic	α Al_2O_3 + Cristobalite + Phase X
7	E-18 As-sintered--Plastic	α Al_2O_3 + Cristobalite + Phase X
12	Al_2O_3 + H_3PO_4 --reacted	α Al_2O_3 + Quartz
11	Fisher AlPO_4	Amorphous
8	E-18 As-reacted 3 hours	α Al_2O_3 + Amorphous
9	E-18 As-reacted 2 hours	α Al_2O_3 + Amorphous
10	E-18 As-reacted 3 hours	α Al_2O_3 + Amorphous
14	Al_2O_3 + 10% Co_3O_4 + H_3PO_4 As-reacted	α Al_2O_3 + Amorphous + Quartz
15	Al_2O_3 + 10% Co_3O_4 + H_3PO_4 As-reacted	α Al_2O_3 + Quartz
18	Al_2O_3 + 2 1/2% Co_3O_4 + H_3PO_4 As-reacted	α Al_2O_3 + Quartz
19	Al_2O_3 + 5% Co_3O_4 + H_3PO_4 As-reacted	α Al_2O_3 + Quartz

TABLE VII. RESULTS OF X-RAY DIFFRACTION
STUDIES, CONT'D.

Specimen No.	Specimen	Phases Present in the Specimen
20	$\text{Co}_3\text{O}_4 + \text{H}_3\text{PO}_4$ --As-reacted	Amorphous
21	$\text{Al}_2\text{O}_3 + 2\% \text{ ZnO} + \text{H}_3\text{PO}_4$ -- As-reacted	$\alpha\text{-Al}_2\text{O}_3 + \text{Quartz}$

TABLE VIII. X-RAY DIFFRACTION DATA FOR SPECIMEN NO. 2

Sample X-Ray Pattern			Reference X-Ray Patterns	
2 θ	d(Angstroms)	Relative Intensity	Phase	d(Angstroms)
14.54°	6.092	31	Amorphous	----
19.44	4.566	18	Amorphous	----
20.58	4.316	8	Quartz form	4.33
21.00	4.230	29	Cristobalite form	4.294
21.66	4.103	28	Cristobalite form	4.102
25.30	3.520	63	α alumina	3.48
26.52	3.361	34	Quartz form	3.393
28.14	3.171	28	Cristobalite form	3.163
29.88	2.990	69	Phase X	----
31.32	2.856	19	Cristobalite form	2.867
34.76	2.581	13	Not identified	----
35.26	2.545	100	α alumina	2.55
35.80	2.508	8	Cristobalite form	2.499
37.90	2.374	44	α alumina	2.38
41.20	2.191	8	Quartz form	2.153
43.48	2.081	99	α alumina	2.08
52.68	1.737	38	α alumina	1.74
56.46	1.630	16	Cristobalite form	1.616
57.60	1.600	68	α alumina	1.60
61.42	1.509	14	α alumina	1.51
66.68	1.402	27	α alumina	1.40
67.88	1.380	8	Quartz form	1.394
68.30	1.373	39	α alumina	1.369
69.48	1.352	9	Not identified	----
77.00	1.238	18	α alumina	1.235
95.34	1.043	15	α alumina	1.042
99.74	1.008	6	α alumina	1.016
101.16	0.998	12	α alumina	0.996

Specimen No. 2 was a brittle as-sintered E-18 test specimen.

TABLE IX. X-RAY DIFFRACTION DATA FOR SPECIMEN NO. 3

Sample X-Ray Pattern			Reference X-Ray Pattern	
2 θ	d(Angstroms)	Relative Intensity	Phase	d(Angstroms)
20.70 ^o	4.291	26	Cristobalite form	4.294
21.80	4.077	33	Cristobalite form	4.102
25.80	3.453	100	α alumina	3.48
29.85	2.993	99	Not identified	----
30.30	2.950	51	Phase X	2.867
35.40	2.536	100	α alumina	2.55
38.00	2.368	58	α alumina	2.38
43.60	2.076	100	α alumina	2.08
52.80	1.734	64	α alumina	1.74
57.00	1.616	15	Cristobalite form	1.616
57.70	1.598	100	α alumina	1.60
58.60	1.575	17	Cristobalite form	1.573
61.40	1.510	18	α alumina	1.51
55.70	1.402	49	α alumina	1.40
68.40	1.372	62	α alumina	1.369
77.20	1.236	33	α alumina	1.235
81.00	1.187	6	α alumina	1.187

Specimen No. 3 was a plastic as-sintered E-18 test specimen.

TABLE X. X-RAY DIFFRACTION DATA FOR SPECIMEN NO. 12

Sample X-Ray Pattern			Reference X-Ray Patterns	
2 θ	d(Angstroms)	Relative Intensity	Phase	d(Angstroms)
20.50°	7	4.330	Quartz form	4.33
20.77	14	4.227	Cristobalite form	4.294
21.84	94	4.069	Cristobalite form	4.102
25.60	52	3.480	α -alumina	3.48
26.44	61	3.371	Quartz form	3.393
28.24	10	3.160	Cristobalite form	3.163
31.20	10	2.867	Cristobalite form	2.867
35.20	100	2.550	α -alumina	2.55
35.82	10	2.508	Cristobalite form	2.499
37.80	28	2.380	α -alumina	2.38
43.38	77	2.086	α -alumina	2.08
46.64	4	1.947	Cristobalite form	1.94
48.18	4	1.889	Cristobalite form	1.89
49.66	5	1.871	Quartz form	1.839
52.60	35	1.740	α -alumina	1.74
57.54	80	1.602	α -alumina	1.60
59.70	5	1.549	Quartz form	1.559
61.34	10	1.511	α -alumina	1.511
66.52	23	1.406	α -alumina	1.40
67.32	4	1.391	Quartz form	1.394
68.20	30	1.375	α -alumina	1.369
76.92	17	1.239	α -alumina	1.235

Specimen No. 12 was produced by reacting aluminum oxide with phosphoric acid for two hours at 200°C.

APPENDIX I

RAW MATERIALS

Raw Materials

<u>Material</u>	<u>Supplier</u>
1. Amblygonite	Foote Mineral Company
2. Alumina	Alcoa - A-10
3. Cobalt Oxide	Harshaw Chemical Company (technical grade)
4. Zinc Oxide	Harshaw Chemical Company (reagent grade)
5. Phosphoric Acid	Harshaw Chemical Company (reagent grade, 85%)
6. " N " Fibers	Directorate of Materials and Processes Wright-Patterson Air Force Base, Ohio

APPENDIX II

MEASUREMENT OF THE DAMPING PROPERTIES OF MATERIALS

MEASUREMENT OF THE DAMPING PROPERTIES OF MATERIALS

The dynamic method of determining the modulus of elasticity of a specimen is very accurate at moderate temperatures. Experimental results obtained by this method at high temperatures are poor and hard to interpret. The reason for this is the increased properties of the material at elevated temperatures, which causes the signal impressed on the specimens to be attenuated. To obtain information about the physical properties of the material at elevated temperatures, an apparatus for high temperature damping studies was designed and assembled. This apparatus, in conjunction with equipment which can evaluate an exponential envelope of the decaying oscillation, can also be used to determine the internal friction and other rheological properties of the oxide-phosphate bonded materials. Thus, it is possible that it can be used as a micro-structural research tool to determine the mechanism of plastic deformation.

The equipment used to study the damping of the samples is almost the same as that used for dynamically measuring the modulus of elasticity. The difference is that in the dynamic test the specimen is vibrated for only a very short time, so that after the pulsing the resultant damping of the impressed signal can be observed on an oscilloscope. Hence, an electronic circuit is needed which will control the time that the signal is impressed on the specimens, and will also produce a pulse which will trigger the sweep oscillator in the oscilloscope at the same time that the specimen is pulsed.

The device used to gate the driver is simply a plate operated relay triggered by a relaxation oscillator. As the temperature of the sample is increased, it will be necessary to pulse the sample at a greater rate. This is accomplished by changing the time constant of the relaxation oscillator.

The presentation on the oscilloscope should then be the damped oscillation of the sample. To evaluate this decaying oscillation is a far more difficult problem than producing it. This requires an apparatus which can measure the voltage of the decaying sine wave at a specific time interval after the pulsing of the specimen.

First, the circuitry which produces a pulsed input to the driver was designed, built, and tested before designing the evaluation apparatus. The reasons for this were (1) to ascertain whether the circuitry would adequately perform its designated function and (2) to make sure that the oxide-phosphate bonded specimens would not show damping characteristics that were impossible to evaluate.

The results of the tests indicate that the sample pulsing circuit incorporated with the dynamic modulus equipment will produce a damped response when used in conjunction with an oxide-phosphate bonded sample. So an apparatus which will provide the necessary data to evaluate the damped wave has been designed and is now being built.

The first step in determining the damping characteristics of a specimen is to dynamically test it to determine its resonant frequency. Then the oscillator output is switched to a pulsing circuit to provide a tone burst. This tone burst is then fed to the driving mechanism which vibrates the sample and the decaying oscillation is available at the pickup end of the sample. This decaying wave form is the one which is to be evaluated and all necessary control signals are devised from it.

The first circuit in the evaluation apparatus is a square wave oscillator that provides a terminal output of one kilocycle. This square wave is fed into a differentiating circuit that produces a series of positive and negative pulses. After the negative pulses are removed, the remaining positive pulses are sent to the gate tube.

Before the sample is pulsed with its resonant frequency, there is no input to the gate control tube. When the sample does receive this tone burst, the decaying oscillation then appears on the gate control grid and opens the gate. This "open gate" condition will last so long as there is a signal of a predetermined level on the grid. Actually the gate closes when the damped signal decays to what is effectively zero.

As soon as the gate opens, the decade counting units count the pulses from the square wave generator and stop when the gate closes. The pulses are fed to the fourth counting unit, which then feeds the third counting unit where the pulse repetition rate is divided by ten.

The second and first counting units also divide the pulse repetition rate by ten. So the readings will be in seconds. This is the total decay time.

To evaluate the exponential curve which is in the form of $y = Ke^{-at}$ several amplitude readings at known times (after the pulsing of the sample) are necessary. As it would be extremely difficult to determine the peak amplitude, a method has been devised to obtain the root mean square value of the signal. The peak amplitude can then be obtained by multiplying the root mean square value by 1.414.

From each of the neon indicating lamps in the decade counting unit, an output is taken and fed through a series of selection switches. The switches select the time that the root mean square value of the amplitude will be read. To accomplish this, a series of thyatron is used as a memory circuit. The decaying wave form from the sample, which operates the gating circuit, also goes to a meter. The meter is modified so that the needle will stop when the meter is presented with the proper trigger pulse.

So as the signal amplitude falls, the meter needle falls with it until the time selected by the selector switches is reached and the needle stops. The meter stopping pulse is provided by the thyatron circuit. By making several readings, it will be possible to compute the exponential curve.

<p> Aeronautical Systems Division, Dir/Materials & Processes, Nonmetallic Materials Lab, Wright-Patterson AFB, Ohio. Rpt No. ASD-TDR-62-202, Pt. II. HIGH TEMPERATURE INORGANIC STRUCTURAL COMPOSITE MATERIALS. Final report, Jan 63, 60p., incl illus., tables, 8 refs. Unclassified Report </p> <p> Two phosphate bonded matrix materials for a composite system were studied. Polymorphism of the aluminum phosphate was responsible for wide variance in physical properties of the matrix materials. Corrosion varied as method of processing with wet layup specimens being </p> <p style="text-align: right;">(over)</p>	<p> 1. Composite Materials 2. Refractory Coatings 3. Plastic Coatings 4. Fiber-Reinforced 5. Laminated Plastics I. AFSC Proj 7340, Task 73402 II. Contract No. AF 33(616)-7765 III. Mississippi State Univ., State College, Miss. IV. Not aval fr OTS V. In ASTIA collection </p>
<p> Aeronautical Systems Division, Dir/Materials & Processes, Nonmetallic Materials Lab, Wright-Patterson AFB, Ohio. Rpt No. ASD-TDR-62-202, Pt. II. HIGH TEMPERATURE INORGANIC STRUCTURAL COMPOSITE MATERIALS. Final report, Jan 63, 60p., incl illus., tables, 8 refs. Unclassified Report </p> <p> Two phosphate bonded matrix materials for a composite system were studied. Polymorphism of the aluminum phosphate was responsible for wide variance in physical properties of the matrix materials. Corrosion varied as method of processing with wet layup specimens being </p> <p style="text-align: right;">(over)</p>	<p> 1. Composite Materials 2. Refractory Coatings 3. Plastic Coatings 4. Fiber-Reinforced 5. Laminated Plastics I. AFSC Proj 7340, Task 73402 II. Contract No. AF 33(616)-7765 III. Mississippi State Univ., State College, Miss. IV. Not aval fr OTS V. In ASTIA collection </p>
<p> more corrosive and dry pressed specimens being least corrosive. </p> <p> Boron fibers were investigated as a possible reinforcement material. Boron fibers were more corrosive resistant than glass fibers, but also were more brittle, presenting a processing problem. Microscopic examination of the fibers revealed several interesting structural habits of these fibers. Strength properties of the composites were determined on an automatic stress-strain apparatus designed and built specifically for that purpose. </p> <p> This report has been reviewed and is approved. </p> <p style="text-align: right;">(over)</p>	<p> more corrosive and dry pressed specimens being least corrosive. </p> <p> Boron fibers were investigated as a possible reinforcement material. Boron fibers were more corrosive resistant than glass fibers, but also were more brittle, presenting a processing problem. Microscopic examination of the fibers revealed several interesting structural habits of these fibers. Strength properties of the composites were determined on an automatic stress-strain apparatus designed and built specifically for that purpose. </p> <p> This report has been reviewed and is approved. </p> <p style="text-align: right;">(over)</p>
<p> more corrosive and dry pressed specimens being least corrosive. </p> <p> Boron fibers were investigated as a possible reinforcement material. Boron fibers were more corrosive resistant than glass fibers, but also were more brittle, presenting a processing problem. Microscopic examination of the fibers revealed several interesting structural habits of these fibers. Strength properties of the composites were determined on an automatic stress-strain apparatus designed and built specifically for that purpose. </p> <p> This report has been reviewed and is approved. </p> <p style="text-align: right;">(over)</p>	<p> more corrosive and dry pressed specimens being least corrosive. </p> <p> Boron fibers were investigated as a possible reinforcement material. Boron fibers were more corrosive resistant than glass fibers, but also were more brittle, presenting a processing problem. Microscopic examination of the fibers revealed several interesting structural habits of these fibers. Strength properties of the composites were determined on an automatic stress-strain apparatus designed and built specifically for that purpose. </p> <p> This report has been reviewed and is approved. </p> <p style="text-align: right;">(over)</p>

DISTRIBUTION LIST

DEPUTY FOR TECHNOLOGY (ASR) APPLIED RESEARCH REPORTS

ASNE
ASNY
ASNV
ASNG
ASNL
ASNR
ASND
ASNN
ASNP
ASNC
ASNS
ASNX
ASRE
ASRO
ASRS
ASRN
MRO
ASO
AST
ASZ

ASEP
ASRCE
ASREE
ASREA
ASREM
ASREM-1A
ASROM
ASRCN
ASRCNC
ASRCNC-1
ASRCNC-2
ASRCNE
ASRCNL
ASRONP
ASROOP
ASRCP
ASRCT
ASRMT
ASRMP
ASRNE
ASRNG
ASRNR

The above organizations should be addressed as follows:

ASD (AS- - -)
Wright-Patterson AFB, Ohio